

RESEARCH ARTICLE

Multidimensional effects of history, neighborhood, and proximity on urban land growth: A dynamic spatiotemporal rolling prediction model (STRM)

Yingjian Ren¹  | Jianxin Yang^{1,2} | Yang Shen³ | Lizhou Wang⁴ |
Zhong Zhang¹  | Zibo Zhao¹

¹Department of Land Resource Management, School of Public Administration, China University of Geosciences, Wuhan, China

²Key Laboratory of the Ministry of Natural Resources for Research on Rule of Law, Wuhan, China

³College of Management, Gansu Agricultural University, Lanzhou, China

⁴Wuhan Planning & Design Institute (Wuhan Transportation Development Strategy Institute), Wuhan, China

Correspondence

Jianxin Yang, Department of Land Resource Management, School of Public Administration, China University of Geosciences, Wuhan 430074, China.
Email: yangjianxin@cug.edu.cn

Funding information

National Natural Science Foundation of China, Grant/Award Number: 42101275; Fundamental Research Funds for the Central Universities, China University of Geosciences, Grant/Award Number: CUGL170408 and CUGGG-2021; Provincial Natural Science Foundation of Hubei, China, Grant/Award Number: 2023AFB651

Abstract

Accurate prediction of future urban land demand is essential for effective urban management and planning. However, existing studies often focus on predicting total demand within an administrative region, neglecting the spatiotemporal heterogeneities and interrelationships within its sub-regions, such as grids. This study introduces a dynamic spatiotemporal rolling prediction model (STRM) that integrates historical trends, neighborhood status, and spatial proximity for spatially explicit prediction of urban land demand at a grid level within an administrative region. STRM leverages historical urban land demand and proximity information from neighborhood grids to predict future demand of the foci grid. By integrating history and neighborhood information into a deep forest model, STRM provides an approach for rolling predictions of grid-level urban land demand. Parameter sensitivity and structural sensitivity analyses of STRM reveal the impact of historical lags, neighborhood size, and spatial proximity on urban land demand predictions. Application of STRM in Wuhan demonstrated the performance of STRM over a 17-year period (2000–2017), with an average adjusted R^2 of 0.89, outperforming other urban land demand prediction models. By predicting demand on a year-by-year basis, STRM effectively captures spatiotemporal heterogeneity and enhances the resolution of urban land demand prediction. STRM represents a shift

from static macroscopic to dynamic microscopic prediction of urban land demand, offering valuable insights for future urban development and planning decisions.

1 | INTRODUCTION

In recent decades, researchers have proposed various models to simulate urban growth and predict future urban development scenarios (Balmaceda & Fuentes, 2016; Batty et al., 2019; Cilliers et al., 2021). These models aim to address urbanization issues such as the heat island effect, landscape fragmentation and biodiversity loss (Gao et al., 2022; Xu et al., 2020; Ye et al., 2015). The growth pattern of urban is influenced by both macro-level urban land demand and micro-level spatial configuration, reflecting bottom-up and top-down regulatory processes, respectively (Aquilué et al., 2017; Ke et al., 2018; van Vliet et al., 2017). Due to differences in biophysical, socioeconomic conditions, and historical urban development trends, urban land demand exhibits spatiotemporal heterogeneity across different sub-regions within a city (Yang, Tang, et al., 2023; Zhou et al., 2020). Although recent studies have utilized statistical models and machine learning methods to estimate annual urban land demand, accounting for temporal variations, they often overlook the granular spatial heterogeneity of urban land demand within subregions (Ke et al., 2015; Noszczyk, 2018).

Spatiotemporal variations in urban land demand significantly influence the pattern and form of urban structure (van Vliet et al., 2017). Considering the spatial heterogeneity of urban land demand is crucial for accurately simulating urban landscape patterns and changes. Effective methods to account for this heterogeneity include spatially dividing the study area into low-level administrative units or using clustering methods to partition the area into irregular sub-regions (Engelen et al., 2007; Schneider & Woodcock, 2008). However, these methods often treat sub-regions as independent entities, neglecting their spatial connections and interactions in urban development activities. Urban growth is a geographical phenomenon characterized by both temporal and spatial attributes. The historical context and development conditions of neighboring areas, along with regional proximity, are key factors affecting urban land demand (Tepe, 2023). Historical urban growth trends and current development conditions influence both present and future urban growth. Incorporating historical urban growth information into simulations, such as through auto-correlation analysis, has been shown to enhance simulation and prediction accuracy of urban growth (Nahuelhual et al., 2012). Moreover, urban growth processes often exhibit spatial dependence and feedback between neighborhoods, with many studies demonstrating the impact of spatial dependencies on model performance. The self-organizing nature of urban growth suggests that growth in specific city areas is influenced not only by historical trends but also by the development trends of surrounding areas. This self-organizing feature provides theoretical support for simulating heterogeneous urban land demand by incorporating spatiotemporal dependency and neighborhood interactions.

This study proposes a spatiotemporal rolling prediction model (STRM) to address gaps in current urban land demand prediction models. STRM considers the impacts of spatiotemporal lag effect and spatial proximity on urban land demand. By a set of spatiotemporal parameters that represent spatiotemporal lags and spatial proximity, STRM can predict grid-level urban land demand annually. These spatiotemporal parameters are calibrated through parameter and structure sensitivity analysis to enhance model performance. Based on these calibrated parameters, STRM provides reliable predictions of future urban land demand.

The application of STRM in Wuhan, China, demonstrates its potential to support urban land development and planning decisions. STRM aids decision-makers in better responding to urban development challenges, offering insights into the dynamic patterns and influencing mechanisms of urban growth, thereby providing more scientific and reliable support for urban planning and management decisions. The key scientific questions addressed in this

study are: (1) Can spatiotemporal lag in urban development and proximity information depict the spatiotemporal heterogeneity of grid-level urban land demand? (2) Can the proposed STRM effectively predict future urban land demand using spatiotemporal lag and proximity information?

2 | LITERATURE REVIEW

2.1 | Urban land demand predicts based on the CA framework

Urban growth simulation models developed based on CA have gained widespread adoption for their capability to simulate dynamic geographical phenomena through the incorporation of neighboring interactions (Cilliers et al., 2021; Stanilov & Batty, 2011). For instance, CLUE-S (Verburg et al., 2003), UrbanSim (Waddell, 2007), FUTURE (Meentemeyer et al., 2013), SLEUTH (Osman et al., 2016), FLUS (Liu et al., 2017), and PLUS (Liang et al., 2021) are designed to analyze and simulate dynamic urban changes, habitat evolution, and predict future urban growth patterns (Fisher-Gewirtzman & Blumenfeld-Liberthal, 2013; Tang et al., 2021; Yang et al., 2020).

These CA-based models follow a process consisting of two main procedures at the macro level, namely demand prediction and space allocation (Aquilué et al., 2017). Predicting demand is often a prerequisite for spatial allocation, estimating the quantity of future urban growth. Researchers have conducted extensive research on “how to define urban land spatial allocation rules”, because this issue is the key to distinguishing the simulation performance of CA models. From the aspects of neighborhood configuration (Moore or von Neumann neighborhoods), representation of spatial objects (polygons, regular grids, or patches) and randomness (usually achieved through Monte Carlo simulations), many improved conversion rules are proposed to make the simulated urban land landscape pattern more realistic (Liao et al., 2016; Mustafa et al., 2018; Zhai et al., 2020). However, researchers often neglect the improvement of the demand predicting part.

In terms of demand predicting, it mainly includes static and dynamic methods. Static methods include regression analysis, trend fitting, and neural networks, which are used to establish the connection between the quantity of urban land and indicators such as population size, economic development, and industrial structure (Chen et al., 2014; Li & Yeh, 2001; Wu, 1997). Typical urban development models of this kind are RF-CA, ANN-CA and logistic-CA (Liu et al., 2023; Wang & Wang, 2022; Xu et al., 2021). Dynamic methods utilize models like system dynamics to express the dynamic feedback between policy, socioeconomic conditions and the quantity of urban land (Zhang et al., 2024). The urban land demand predicted by these models is further input into the spatial allocation module to guide the micro-processes of urban land simulation from a macro perspective. To enhance the spatial allocation process, it is essential to optimize urban expansion simulation models with a focus on urban land demand. Similar to the spatial allocation process, current methods of predicting urban land demand over multiple years often neglect temporal differences in demand. Additionally, methods that predict large-area demand frequently overlook the interactions between subregions. External models used to estimate urban land demand not only fail to account for spatiotemporal variations but also exhibit weak integration with the spatial allocation process. Consequently, these models do not effectively utilize spatialized urban land demand as a critical guiding factor (Cunha et al., 2021; Liu et al., 2020).

2.2 | Heterogeneity of urban land demand

Urban land demand at the macro level often fluctuates in response to economic development and population changes (Zhou et al., 2020). For instance, during periods of rapid economic growth and population expansion, the demand for urban land increases, whereas it decreases during economic downturns. Typically, a set of time series

data is employed to predict annual urban land quantities through statistical analysis or machine learning methods (Chen et al., 2019; Yang, Sun, et al., 2023). To capture temporal differences in urban land demand, a straightforward method is to use year-by-year estimates (Liu et al., 2020), which are then spatialized by specific allocation modules within urban growth simulation models.

However, urban land demand estimated using traditional models often fails to adequately address temporal and spatial variations. The spatiotemporal heterogeneity of urban land demand highlights geographical differences in urban development across different subregions within a city over time (Yang, Tang, et al., 2023). This demand is not uniformly distributed; it is typically higher in economically thriving and densely populated areas, such as urban centers, near commercial hubs, or in new development zones. Conversely, in remote towns and villages away from urban cores, the demand for urban land is generally lower. This uneven distribution both directly and indirectly influences the spatial allocation process, thereby shaping the landscape pattern of urban expansion (Morrill, 1970).

To address the spatial heterogeneity of urban land demand, modelers have traditionally divided study areas into administrative districts for urban expansion simulations at global, national, or economic zone scales, partitioning regions into countries, cities, and counties (Engelen et al., 2007; Huang et al., 2021). This approach often employs statistical relationships between socioeconomic factors and urban land development to estimate demand across large-scale regions. While effective for simulating the impact of different policy scenarios, this method can disrupt the spatial continuity of geographical elements subjectively.

At the city scale, researchers have developed various spatial partitioning methods to accommodate the heterogeneity of demand. For example, dividing a city into smaller administrative units—cities into counties, and counties into towns—allows for a more detailed consideration of urban land demand at different administrative levels (Seto et al., 2012). Although the heterogeneity of urban land demand at different administrative levels is considered, this approach may overlook subtle policy differences across these levels. Additionally, some researchers have adopted spatial clustering methods to segment the study area into irregular zones based on homogeneity in socioeconomic characteristics (Ke et al., 2015). While this method ensures that socioeconomic backgrounds are consistently represented, acquiring spatialized socioeconomic data in irregular areas poses significant challenges. Another division strategy involves establishing concentric rings from the city center outward, categorizing the city into regular zones (Ahasan & Güneralp, 2022; Yang, Sun, et al., 2023). This model accounts for micro-physical changes in urban land demand over time and aligns well with micro-urban dynamics, facilitating integration with spatial allocation processes. However, it is primarily suited to plain urban areas that expand outward from the city center and may not adequately capture the complex interactions among different urban zones.

2.3 | Spatiotemporal lag effect and proximity in urban growth

Previous research has extensively demonstrated the effectiveness of data-driven empirical methods in simulating urban growth processes (Fu et al., 2018; Lauf et al., 2012; Losiri et al., 2016). Urban development suitability maps, an essential input to the spatial allocation process, are typically created by establishing regression relationships between urban development and various biophysical and socioeconomic factors (Castella & Verburg, 2007). These relationships significantly influence the effectiveness of simulation results by impacting the transition rules used in the models (Liang et al., 2021). However, many studies also highlight the importance of historical development trends, neighborhood relationships, and proximity determined by distance factors as critical elements in predicting urban land demand (Deng & Srinivasan, 2016; Ferdous & Bhat, 2013; Iacono et al., 2008).

Including historical development trends in urban land demand estimates is crucial due to the inertial mechanism of urban development, where future urban land development is influenced by past activities (Nahuelhual et al., 2012; Tepe & Guldmann, 2020). However, changes in urban development may exhibit a temporal lag, becoming apparent only after a significant period (Bhat et al., 2015; Huang et al., 2009). Effectively accounting for dynamic changes in historical development in regression models can significantly improve the simulation of

large-scale land use changes (Tepe & Guldmann, 2017, 2020). For instance, incorporating data from lagged periods into a logistic autoregressive model can accurately capture the nonlinear dynamics of urban development (Tepe & Guldmann, 2020).

Neighborhood relationships also play a critical role in simulating urban growth, particularly in influencing the neighborhood effect in CA models. Urban land demand is generally higher in areas adjacent to already urbanized regions, in line with the first law of geography (Goodchild, 2004; Tobler, 2004). Urban development typically spreads outward from urban centers, connecting new urban areas to existing ones. This spatial diffusion of urban growth, with its pronounced lag effect, prioritizes land closest to urbanized areas for development. Conversely, regions like distant suburbs have a lower likelihood of urban development.

Additionally, distance-related variables are crucial for representing spatial proximity, and they play a vital role in regulating auto-correlation and heterogeneity in spatial modeling. Researchers have explored the potential of using these variables or rules to better understand urban development phenomena (Arsanjani et al., 2013; Liao & Wei, 2014; Ou et al., 2017). Proximity to urban centers, key infrastructure, important transportation hubs, and already urbanized areas typically correlates with increased socio-economic activities and higher population density, thereby escalating urban land demand. Furthermore, examining the interplay between scale and proximity is fundamental for understanding urban land patterns. Researchers also investigate this relationship to discuss how proximity influences urban land use patterns across different scales, highlighting its critical role in spatial dynamics (Munroe & Müller, 2007; Li et al., 2022).

Although urban land demand estimates based on traditional models consider temporal and spatial divisions, as well as the effects of spatiotemporal lag and proximity, they still estimate demand independently for each area. This approach often fails to account for the varied impacts of environmental changes, such as historical trends and neighborhood conditions, across different regions. Therefore, effectively capturing spatiotemporal heterogeneity requires predictions of urban land demand that integrate historical trends, neighborhood status, proximity, and the interactions among areas at various scales. This comprehensive approach ensures a more accurate reflection of complex urban dynamics.

3 | MATERIALS AND METHODS

3.1 | Study area

The study area is Wuhan, located in Hubei Province, China, situated between 113°41' E-115°05' E and 29°58' N-31°22' N. Positioned in the eastern part of the Jiangnan Plain and within the middle reaches of the Yangtze River, Wuhan covers an area of 8569.15 km². This region is notably marked by the convergence of the Yangtze and Han Rivers in its central areas, a unique geographical feature that has significantly influenced its urban development (see Figure 1). From 2010 to 2020, Wuhan's permanent population increased from 9.7853 million to 12.4477 million, a rise of 27.21%, while its built-up area expanded from 475 to 812.39 km², an increase of 71.03% (China S. S. B., 2010, 2020). This rapid expansion of urban land has outpaced population growth, presenting various urban challenges. Addressing these issues necessitates scientific regulation to effectively manage Wuhan's future urbanization paths. Therefore, conducting a spatiotemporal demand prediction for urban land growth in Wuhan is essential for promoting sustainable urbanization.

3.2 | Data and preprocessing

Urban land data for the study area, covering the period from 1990 to 2017, were interpreted by Gong Peng using the Google Earth Engine (GEE) platform, which utilized Landsat satellite images and auxiliary data. The overall

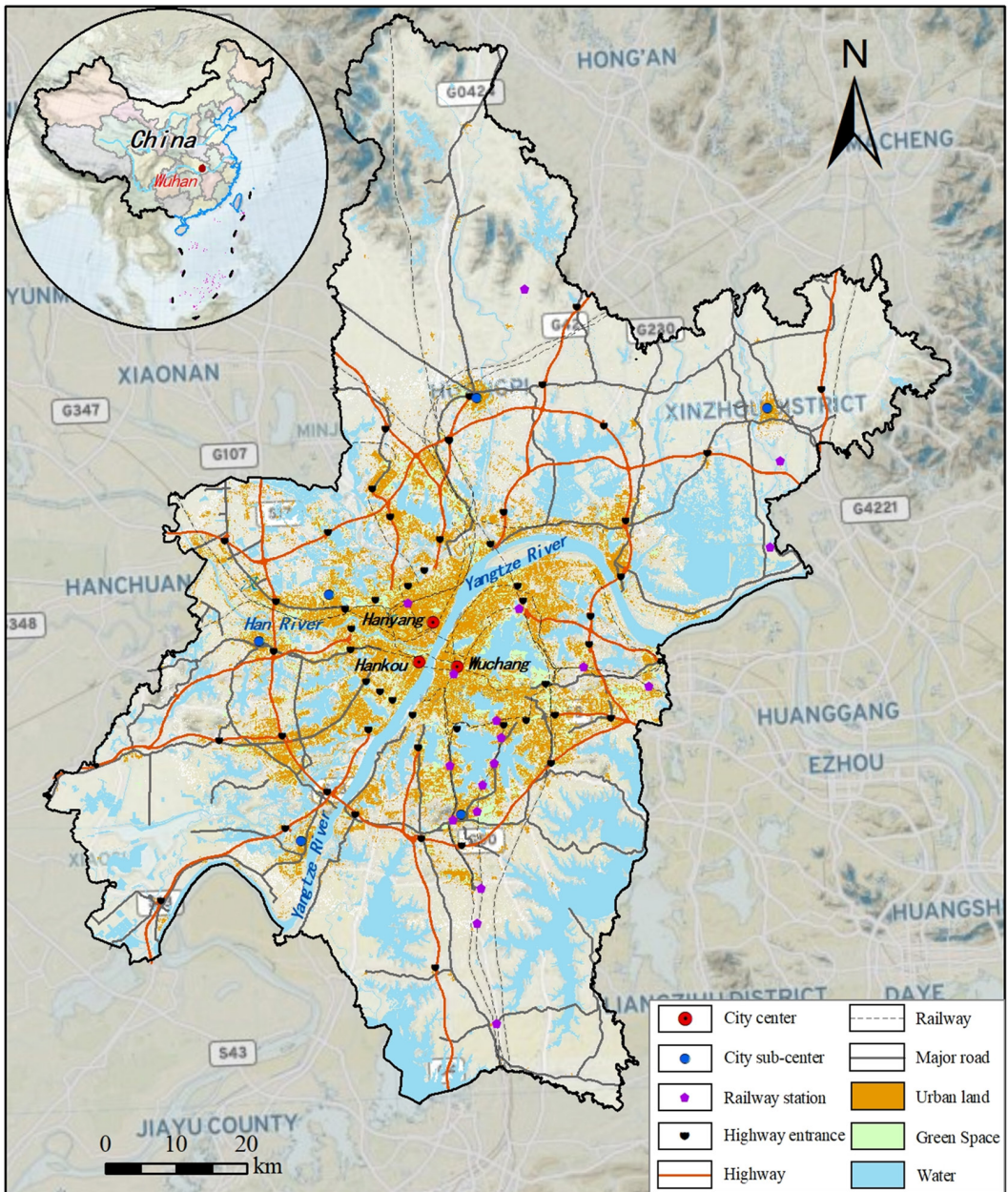


FIGURE 1 Location of the study area (Wuhan City, Hubei Province, China).

interpretation accuracy exceeds 90% (Gong et al., 2020). Water bodies in the study area were extracted from the global land use/land cover data in 2020 produced by ESRI. Additionally, this study identified ten environment variables that potentially influence urban land development. The data sources and calculation methods for these variables are detailed in Table 1.

The study area is divided into regular grids, and urban land demand of each grid is defined as the proportion of urban land area in the grid with water bodies excluded:

TABLE 1 Data sources and calculation methods.

Type	Environment variables	Original data	Data sources	Calculation method
Biophysical variables	Altitude (x_1)	DEM	Geospatial data cloud (https://www.gscloud.cn)	Computing the mean value for each grid.
	Slop (x_2)	Slop		
Distance-driven variables	Distance to city center (x_3)	City center	Referring to the method proposed by Chen et al. (2019) to determine	Computing Euclidean distances in ArcGIS 10.7 and calculating the mean within each grid.
	Distance to city sub-center (x_4)	City sub-center		
	Distance to town center (x_5)	Town center		
	Distance to water (x_6)	Major water	Global land use/cover data published by ESRI (https://livingatlas.arcgis.com/landcover)	
	Distance to river (x_7)	Yangtze and Han River		
	Distance to highway entrance (x_8)	Highway entrance	National Centre for Basic Geographic Information (https://www.ngcc.cn)	
	Distance to railway station (x_9)	Railway station		
	Distance to major road (x_{10})	Major road		

$$\eta(d, t) = \frac{S_b}{S - S_w} = \begin{cases} 1, & \text{if } S_b = S - S_w \text{ or } S_b = S_w = \frac{S}{2} \\ A, & \text{if } S > S_b + S_w, 0 < A < 1, S \geq S_b + S_w, S > 0, S_b \geq 0, S_w \geq 0 \\ 0, & \text{if } S_b = 0 \text{ or } S = S_w \end{cases} \quad (1)$$

where $\eta(d, t)$ represents the proportion of urban land in a grid i with a side length of d at time t (observations), where $0 \leq \eta(d, t) \leq 1$. S represents the area of the regular grid unit, calculated as $d \times d$. S_b represents the area of urban land in the grid unit. S_w represents the area of the water bodies in the grid unit. We assumed that areas other than water bodies all can be converted into urban land. There are grids that are all water bodies, i.e., $S = S_w$. Therefore, to ensure the denominator of Equation (1) is meaningful, the urban land proportion of these grids has been assigned to 0, that is $\eta(d, t) = 0$. These water-filled grids are excluded from further urban land demand prediction.

Figure 2 exemplifies the spatial distribution of the normalized environment variables in Table 1 within a grid of $1 \times 1 \text{ km}^2$ size. Details on how $\eta(d, t)$ and the environment variables were calculated are provided in Appendix A.

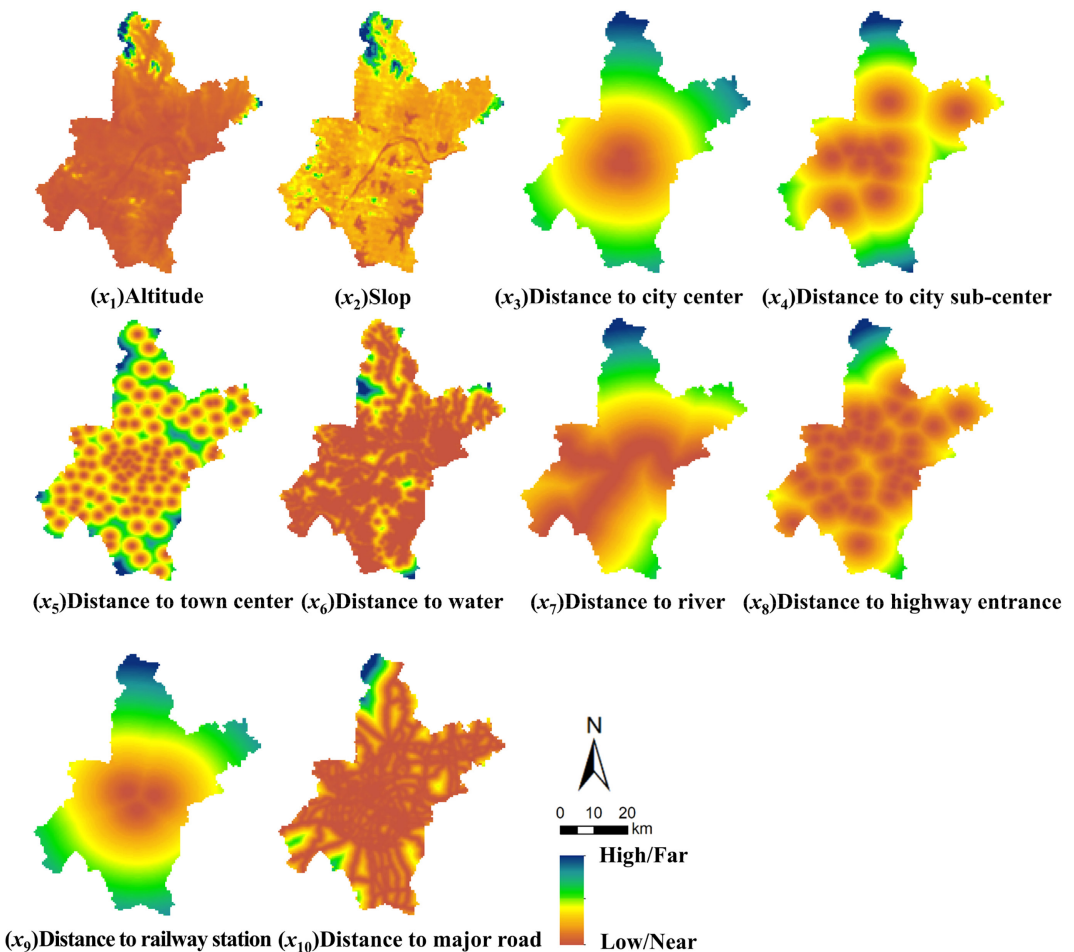


FIGURE 2 Environment variables that influence urban land demand.

3.3 | Spatiotemporal rolling prediction model (STRM) of urban land demand

3.3.1 | Parameters designation in STRM

At time t , urban land demand in grid i is predicted using STRM as Equation (2):

$$q_i(d, t, r) \sim f(Q_{t-1,d,\Omega_r}, Q_{t-2,d,\Omega_r}, \dots, Q_{t-k,d,\Omega_r}; D_{d,i}) \quad (2)$$

where $q_i(d, t, r)$ represents the urban land demand in grid i with side length d at a specific year t , r represents the neighborhood size of the grid, k denotes the lag period ($0 < k \leq T$). T is the maximum lag period ($T = 10$ in this study). Ω_r is the set of grid cells centered at the focal grid i and within the radius r of the Moore neighborhood. Q_{t-k,d,Ω_r} represents a vector composed of the urban land demand in grid units within Ω_r at time $t - k$, and $D_{d,i}$ represents a vector composed of the environment variables in grid i . f represents a mapping function that can be linear regression, neural network, or random forest, etc.

STRM examines the impact of spatiotemporal lag effect and spatial proximity on urban land demand. It assumes that, at any moment, the urban land demand in a grid is influenced by the historical urban land demand within that grid, as well as within a certain neighborhood range, alongside the environment variables of the focal grid. Based on this assumption, a set of parameters (see Table 2) is utilized to characterize the response of urban land demand to different spatiotemporal heterogeneous environment.

In the temporal dimension, a maximum lag period of 10 years is defined, denoted as k . For instance, when the lag period is 10 years, STRM extracts urban land demand data for a historical period of 10 years from the focal grid and the neighborhood grid. In the spatial dimension, five neighborhood sizes (denoted as r) and five grid sizes (denoted as d) are defined. Additionally, the environment variables listed in Table 1 were incorporated into the model as factors of proximity to the focal grid. When the neighborhood of the focal grid extends beyond the boundary of study area, the values of environment variables in these grids outside the study area are set to 0.

It should be noted that when exploring the impact on spatiotemporal demand prediction, proximity includes two aspects: the proximity of the focal grid's own environment variables, as well as the proximity of urban land demand in the surrounding neighborhood, can be uniformly characterized by the size of the scanning window. This will be discussed in detail in Section 4.1.3.

3.3.2 | Quantitatively construct the spatiotemporal input data of STRM

The input data of STRM primarily consist of the urban land demand vector Q from the historical period for both the focal grid and its neighborhood grids, as well as the vector D representing the environment variables of the focal grid alone. Figure 3 illustrates the calculation steps for vectors Q and D . The steps are as follows:

TABLE 2 Parameter design and description in STRM.

Dimension	Parameters	Value range	Unit	Description
Temporal dimension	Lag Period (k)	1, 2, 3, 4, 5, 6, 7, 8, 9, 10	Year	Determines the duration of temporal lags in STRM.
Spatial dimension	Neighborhood Size (r)	0, 1, 2, 3, 4	-	Determines the size of the Moore neighborhood (N), calculated as $N = 2 \times r + 1$, where $r = 0$ indicates no neighborhood, $r = 1$ represents a Moore neighborhood within the 3×3 range, and so on.
	Grid Size (d)	1, 2, 3, 4, 5	km	Represents the size of the grid unit.

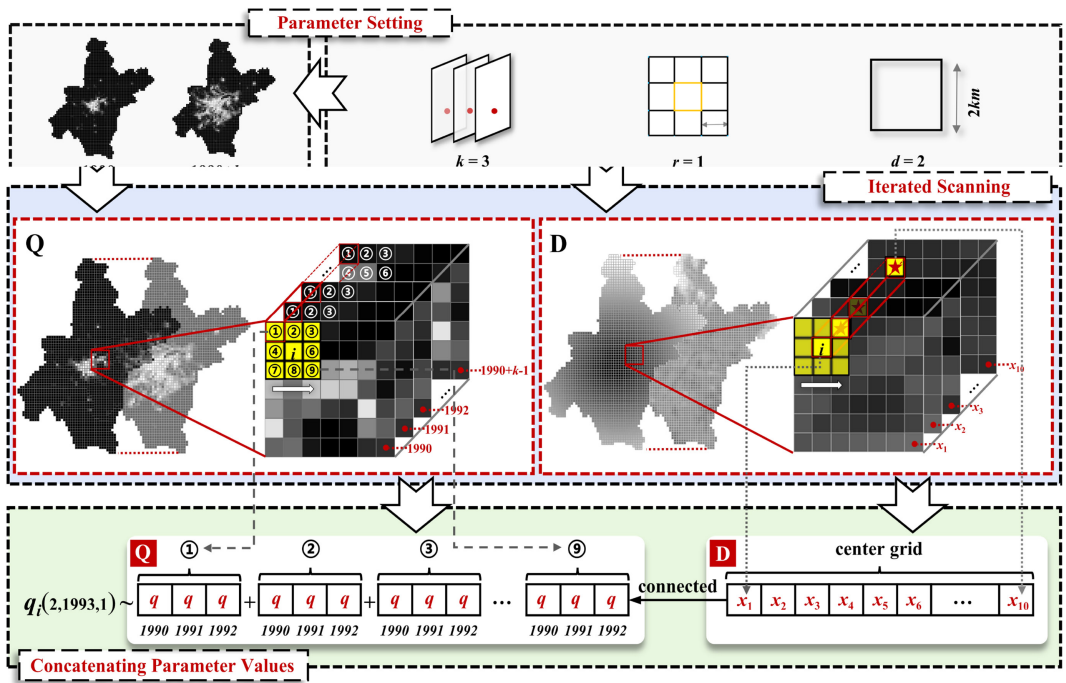


FIGURE 3 Extraction of spatiotemporal neighborhood information.

1. *Parameter setting.* Modelers should set the parameters based on Table 2, including lag period, neighborhood size, and grid size. For example, one can choose a set of parameters as shown in Figure 3, where the lag period is 3 years, the neighborhood size is 3, and the grid size is 2 km.
2. *Iterated scanning.* As shown in Figure 3, assume that the prediction year of the model is $1999 + k$. At this time, a 3×3 scanning window is constructed with a non-empty focal grid i as the center to extract the urban land demand dataset from 1990 to $1999 + k - 1$. Grids that are all occupied by water bodies are excluded from scanning. The scanning window is numbered from ① to ⑨ if the neighborhood size is 3×3 , as exemplified in Figure 3. Data from grid ① in the history years from 1990 to $1999 + k - 1$ forms the first vector. Data from neighborhood grids numbered ② to ⑨ are processed similarly. After completing the neighborhood scanning iteration, STRM concatenates the nine vectors obtained to construct the vector Q for the focal grid i . Vector D is obtained by concatenating the ten environmental factors corresponding to the focal grid i .
3. *Concatenating parameter values.* Connect the vectors Q and D obtained in the previous step to complete the extraction of spatiotemporal information for grid i . The scanning window then moves one grid unit at a time, extracting values from top to bottom and left to right, until it encompasses all grids in the study area. It should be noted that this study also discusses cases where the influence of environment variables is not considered. In such cases, the extraction process for spatiotemporal information does not include the connection of vectors Q and D , the scanning window only fetches the vector Q .

3.3.3 | Mapping function selection and rolling prediction processes

If the environment variables are not included in the prediction process, STRM functions similarly to a spatiotemporal autoregressive model (Harris et al., 2017). However, when these variables are incorporated, STRM

transforms into a structure akin to a mixed spatial autoregressive model (Qin & Lei, 2021). The structure of STRM exhibits significant high-dimensional and complex nonlinear characteristics. For instance, with a neighborhood size of $r = 4$ and a temporal lag of $k = 10$, the model's input vector encompasses 820 elements, calculated as $10 \times (2 \times 4 + 1) + 10$. Traditional spatial statistical models and conventional machine learning models may not be capable of addressing such a complex structure.

Deep learning approaches can well address nonlinear relationships in data, making them capable of capturing spatial second-order relationships and nonlinear associations in geographic data. The deep forest, a deep learning model based on decision trees is one such method initially introduced by Zhou (Zhou & Feng, 2019). This model primarily comprises two components: multi-grained scanning and cascaded forests, which facilitate the comprehensive extraction of feature information from high-dimensional data and efficient management of large-scale datasets. Compared to traditional machine learning approaches, the deep forest model has fewer hyperparameters and offers enhanced training efficiency (He et al., 2018). Therefore, this study chooses to utilize the deep forest model as the mapping function f .

In STRM, the dependent variable, which is urban land demand in a grid, is a continuous variable with values ranging from 0 to 1. Here, 1 indicates that the entire grid is urban land with water bodies excluded, and 0 signifies no urban land within the grid. By extracting spatiotemporal neighborhood information from all grids, we construct the dataset and train the deep forest model to predict future urban land demand for each grid on a rolling basis, as depicted in Figure 4.

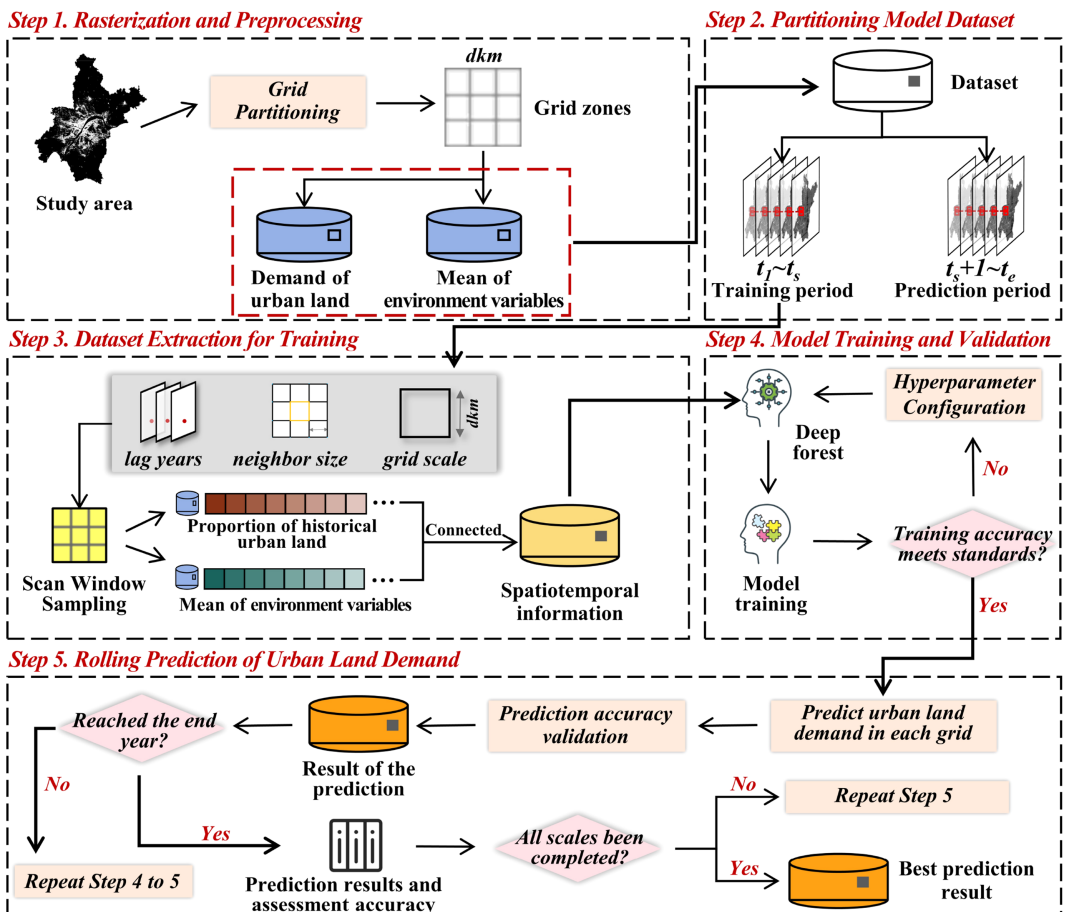


FIGURE 4 Implementation process of STRM model.

The study area is divided into regular grids of size d km. Urban land demand and the averages of environment variables within each grid are calculated annually throughout the study period (1990–2017 in this study). Based on the specified temporal lag k , the study period is divided into a model training period and a model validation period. We assume that t_1 is the initial year (1990 in this study) and t_e is the end year (2017 in this study) for model training and validation in the study area. The beginning year to be predicted is t_s ($t_s = t_1 + k$) in the validation process. For model training, urban land demand within the focal grid of the scanning window serves as the dependent variable. Independent variables include the historical urban land demand of the focal grid and its neighboring grids, as well as the environment variables of the focal grid. Once model training is complete, rolling predictions for urban land demand within each grid for the upcoming years commence as Figure 4. First, STRM utilize data from $t_s, t_s - 1, \dots, t_s - k + 1$ to predict the urban land demand for year $t_s + 1$. Subsequently, STRM incorporates the predicted value for year $t_s + 1$ into the model, together with data from $t_s, t_s - 1, \dots, t_s - k + 2$ to predict the value for year $t_s + 2$. This iterative process continues until the rolling prediction of urban land demand for all grids up to year t_e is completed. The Adjusted R^2 values for the annual predictions are then calculated and recorded. The detailed calculation procedures for Adjusted R^2 are outlined in Equation (S3) in Appendix B. If the model achieves the required validation accuracy, the next steps are initiated. However, if the model underperforms, its parameters are adjusted, and a retraining phase ensues.

4 | PARAMETER AND STRUCTURE SENSITIVITY ANALYSIS OF STRM

4.1 | Parameter sensitivity analysis

4.1.1 | Temporal lags effects in urban land demand

Figure 5, using a grid size of 5 km as an example, illustrates the Adjusted R^2 predicted by the model across all sample lag periods. Appendix C details the effects of temporal lag on model prediction accuracy for various grid sizes. The data from Figure 5 reveal that although the Adjusted R^2 of STRM fluctuates with different neighborhood sizes, there is a consistent overall improvement in prediction accuracy as the lag period increases. Specifically, when the

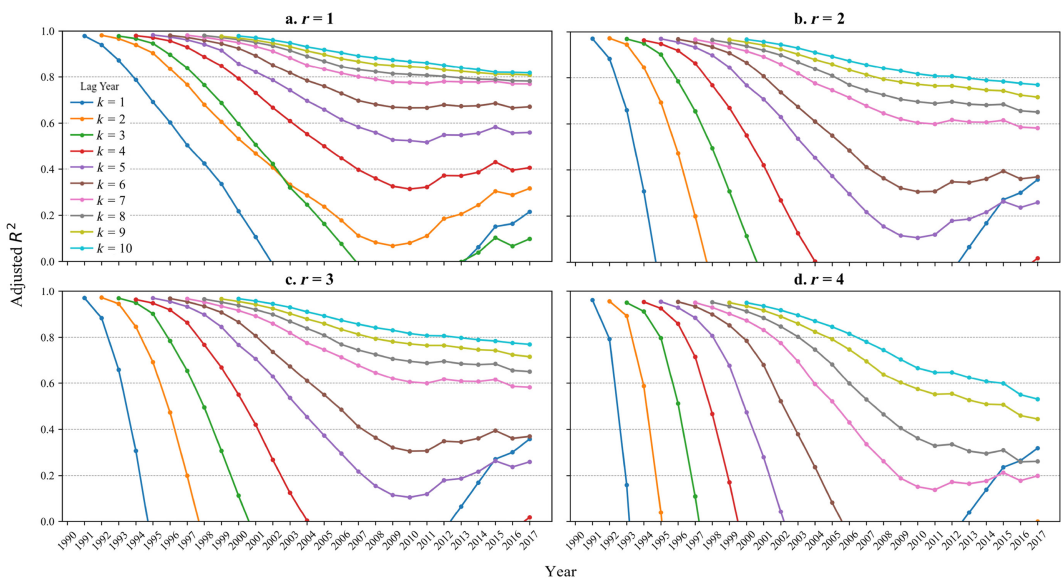


FIGURE 5 Prediction accuracy of STRM model with different lag periods. (a) Moore neighborhood $N = 3$; (b) Moore neighborhood $N = 5$; (c) Moore neighborhood $N = 7$; (d) Moore neighborhood $N = 9$.

lag period extends to 10 years, STRM achieves a notably higher Adjusted R^2 . Additionally, as the neighborhood size expands, the differences in STRM's predictions under various lag periods become more pronounced, with the advantage of a 10-year lag period increasingly evident. In contrast, shorter lag periods, such as 6 years or less, lead to greater fluctuations in STRM's Adjusted R^2 . These fluctuations underscore that longer lag periods enhance STRM's capacity to model the spatiotemporal non-stationarity of urban land demand development. Despite variations in predictive accuracy across different neighborhoods, the data clearly demonstrate that an extended lag period significantly improves STRM's predictive capabilities. This observation corroborates research by Kim et al. (2022), suggesting that incorporating historical urban changes provides insight into the variability of urban growth processes, highlighting the importance of historical lag data for understanding urban land demand dynamics.

4.1.2 | Spatial lags characteristics of urban land demand

According to the temporal lags effects analysis results, we take the optimal lag parameter of 10 years ($k = 10$) as an example to illustrate the Adjusted R^2 of STRM across different neighborhoods and grid sizes (refer to Figure 6). Complete prediction accuracy results under all spatial parameters are detailed in Appendix C. When the neighborhood size is small, for instance, $r = 1$ and $r = 2$, the overall Adjusted R^2 generally increases as the grid size expands. However, with larger neighborhood sizes such as $r = 3$ and $r = 4$, the spatial lags characteristics of STRM exhibits edge effects, causing the Adjusted R^2 to fluctuate with changes in grid size. These observed edge effects, which align with the research by Hu, may be attributed to increased variability in urban land demand across a broader range of neighborhoods (Hu & Lo, 2007). Additionally, with a constant grid size, as the neighborhood size increases, the spatial of the data extracted by the scanning window also expands, leading to a continual decrease in overall Adjusted R^2 . Nevertheless, spatial lags effects (a specific manifestation of spatial dependence), being a localized feature, is subject to a specific distance threshold. According to Tobler's first law of

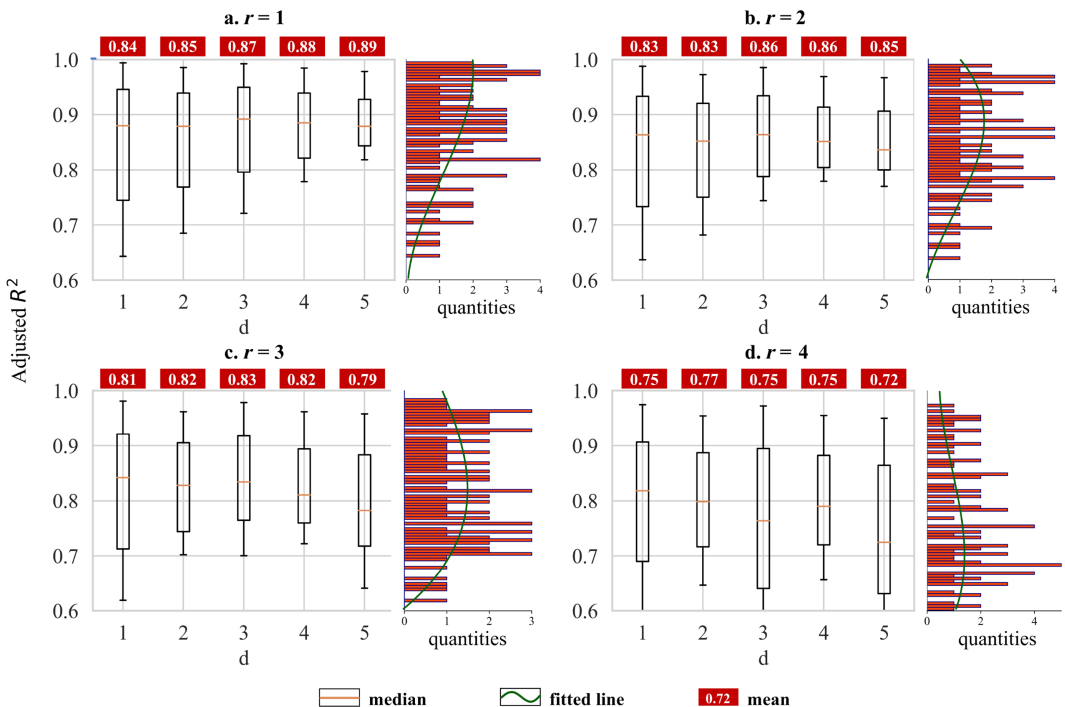


FIGURE 6 Prediction accuracy of STRM model with different neighborhood sizes. (a) Moore neighborhood $N=3$; (b) Moore neighborhood $N=5$; (c) Moore neighborhood $N=7$; (d) Moore neighborhood $N=9$.

geography, spatially proximate locations typically share similar distribution patterns and evolutionary processes (Tobler, 2004). Therefore, an increase in neighborhood size not only leads to considering the impact of more distant urban land demands but also reduces the intensity of spatial interactions. Within the statistical range of all spatial parameters, STRM exhibits the highest prediction accuracy overall when the grid size is 5 km and the neighborhood is configured as 3×3 ($r = 1$).

4.1.3 | Impacts of spatial proximity on urban land demand

The spatial proximity defined in this study includes two aspects. First, the distance between the urban land demand of each grid in the scanning window and the urban land demand of the focal grid. This proximity characterizes the range of neighborhood urban land demand that the focal grid needs to consider. When the neighborhood size r and grid size d change, the range that the scanning window covers will also change. At this point, the neighborhood urban land demand that needs to be considered when predicting urban land demand in the focal grid will change. In addition, this study also incorporates consideration of environment variables in each grid, which include necessary natural limiting variables and distance variables. Therefore, proximity also includes the proximity of each grid to important geographic features (expressed as the mean calculated within the grid). As the grid size d changes, the proximity to important geographic features also changes. Thence, we use a uniform scanning window to explore the impact of proximity on urban land demand prediction. The spatial range of the scanning window is determined by the following equation:

$$S = N \times d = (2r + 1) \times d \quad (3)$$

where S represents the length of the scanning window, which is used to represent the range of spatial proximity (unit: km). r and d represent the neighborhood size and grid size, respectively (see Table 2). The proximity represented by the scanning window is determined by both r and d , so the case when $r = 1$ is not consider.

Figure 7 illustrates the prediction accuracy of STRM across various scanning window sizes. The trend observed is that as the scanning window size increases, prediction accuracy initially rises and then declines. This pattern suggests that beyond a certain proximity threshold, the model begins to incorporate data that is less spatially

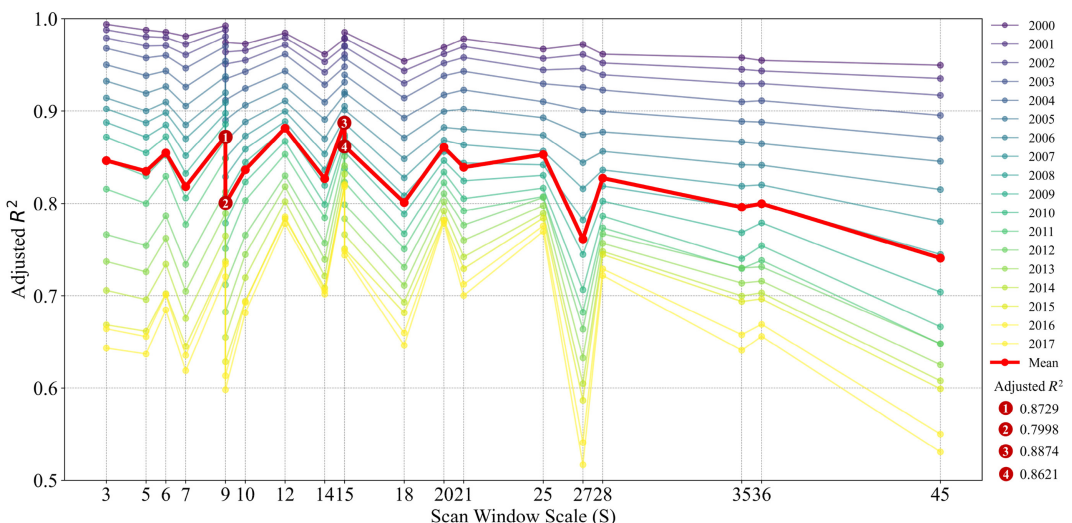


FIGURE 7 Prediction accuracy of STRM model with different scanning window scales from 2000 to 2017. Point 1: $r = 1$, $d = 3$ km; point 2: $r = 4$, $d = 1$ km; point 3: $r = 1$, $d = 5$ km; point 4: $r = 2$, $d = 3$ km.

correlated and more heterogeneous, adversely affecting the prediction outcomes. Additionally, the mean curve for Adjusted R^2 in [Figure 7](#) indicates that the prediction accuracy peaks at $S = 9$ for near-term years (2000–2009), and at $S = 15$ for long-term years (2010–2017). Also note that both $S = 9$ and $S = 15$ scenarios encompass two spatial scale parameters. However, both high-accuracy results (point 1 and point 3) occur at $r = 1$, reaffirming the result that smaller neighborhoods may yield higher prediction accuracy.

4.2 | Structure sensitivity analysis

4.2.1 | Simulation experiments design

To further investigate the impact of each spatiotemporal parameters and environment variables on model performance, eight simulation experiments were designed in this study (refer to [Table 3](#)) to analyze the structure sensitivity of STRM. It has been demonstrated that incorporating a lag period can improve prediction accuracy. Therefore, we have uniformly set the lag period of the input data to 10 years. To validate the impact of the neighborhood, we set up scenarios with ($r = 1$) and without the neighborhood ($r = 0$). Based on the analysis of spatial proximity, we divided the prediction period into near-term and long-term years, each corresponding to different optimal grid sizes ($d = 3$ and $d = 5$). Additionally, we set up scenarios without incorporating environment variables to facilitate the validation of their impact.

4.2.2 | Experiments simulation and analysis

[Figure 8](#) illustrates changes in model accuracy for different simulated experiments outlined in [Table 3](#). In comparison of the Adjusted R^2 for near-term years, NRA and NRE consistently outperform WRA and WRE, with NRA consistently surpassing NRE, and WRA consistently exceeding WRE ([Figure 8a](#)). This indicates that excluding neighborhood information and incorporating environment variables can improve the performance of STRM in simulating urban land demand of near-term years. In the analysis of Adjusted R^2 for long-term years, the inclusion of environment variables consistently enhances model performance ([Figure 8b](#)). However, when simulating years from 2013 to 2017, the consideration of neighborhood information significantly improves model performance. Overall, the four experiments for near-term years (NRA, NRE, WRA, and WRE) and the two experiments for long-term years (WFA and WFE) exhibit relatively stable trends, while the two

TABLE 3 Simulation experiments design of model.

Experiments name	Neighborhood	Prediction period	Grid size (d)	Environment variables	Name explanation
WRA	✓	2000–2009	3 km	✓	W is for including the neighborhood, and N
WFA	✓	2010–2017	5 km	✓	is for eliminating the neighborhood.
WRE	✓	2000–2009	3 km	×	R is the predict for the near
WFE	✓	2010–2017	5 km	×	term, and F is the predict
NRA	×	2000–2009	3 km	✓	for the long term.
NFA	×	2010–2017	5 km	✓	A is for including
NRE	×	2000–2009	3 km	×	environment variables,
NFE	×	2010–2017	5 km	×	and E is for eliminating
					environment variables.

experiments without the consideration of neighborhood information for long-term years (NFA and NFE) show more significant fluctuations. Therefore, the exclusion of neighborhood information may be more suitable for simulating near-term years, while the inclusion of neighborhood information is more appropriate for simulating long-term years. Additionally, the inclusion of environment variables consistently improves model simulation accuracy across all periods.

Figure 9 illustrates the spatial distribution of urban land demand under different simulated experiments. Comparative analysis reveals that the four simulated experiments for near-term years consistently align with observed values at the landscape level ($Adjusted R^2 > 0.88$). Significantly, the simulation results of WRA and WRE exhibit a higher level of aggregation in the central urban area, resulting in larger deviations from actual values. In simulation of long-term years, the results of NFE and NFA depict a spatial concentration of urban land demand in the central urban area, which are more like the observed patterns. However, the WFA and WFE experiment leads to an over-aggregation of high-value areas in the central urban zone, due to the consideration of neighborhood factors, which are significantly deviate from the actual distribution. In summary, considering environment variables will simulate a more diffused distribution of urban land demand, which is suitable for simulating development zones or newly built urban areas. And the inclusion of neighborhood information tends to aggregate high-value areas near existing urban land demand, making it more suitable for simulating large cities and metropolitan areas with a certain larger amount of urban development.

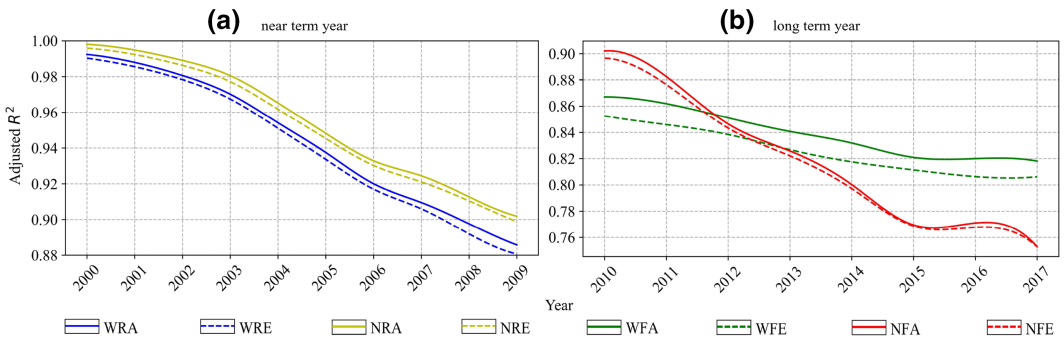


FIGURE 8 Changes in model prediction accuracy in near-term years (a) and long-term years (b).

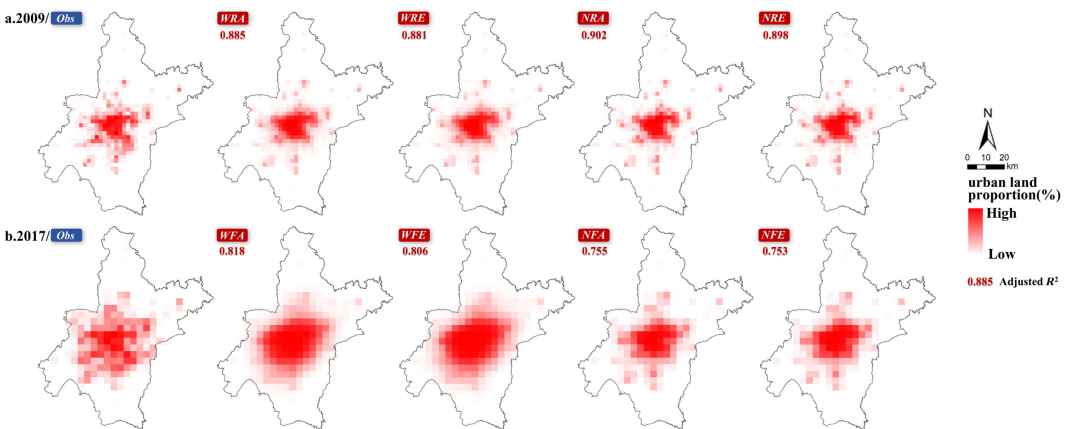


FIGURE 9 Comparison of observed (Obs) values and simulated values in different simulation experiment. (a) Comparison of four predict results with observations for near-term year (2009); (b) Comparison of four predict results with observations for long-term year (2017).

5 | MODEL COMPARISON AND IMPLEMENTATION

5.1 | Validation of STRM model

Based on the parameter and structure sensitivity analysis, optimized parameters of STRM for predictions in near-term years and long-term years are identified (see [Table 4](#)). The predicted spatial distribution of urban land demand for near-term years and long-term years using these parameters are compared with the observed values, as shown in [Figure 10](#). Details on the simulation accuracy using these optimized parameters are documented in [Appendix D](#).

[Figure 10](#) highlights three zoomed-in areas, representing spontaneous growth, filling growth, and edge growth, respectively. In prediction results of near term years, all three cases of urban growth exhibit a high degree of similarity (see [Figure 10a](#)). For predictions of long-term years, both spontaneous and edge growth patterns are similar to the observed values. Nevertheless, by integrating historical context, neighborhood dynamics, and proximity factors, the scanning window can capture spatiotemporal homogeneity across regions, which inevitably leads to proximity effect and distance decay phenomenon. As a result, the predicted urban land demand tends to concentrate around existing urbanized areas, a trend that becomes more pronounced with each subsequent year of rolling predictions. However, this clustering does not impair the model's predictive ability regarding future urban land demand, because consistent with previous studies, urban land demand is anticipated to shift towards more intensive use. This highlights the practicality of this study in utilizing historical context, neighborhood dynamics, and proximity considerations to accurately model future urban land demand.

5.2 | Comparison of different prediction models for urban land demand

To further validate the predictive capabilities of STRM, this study engages several widely recognized urban land quantity prediction models for a comparative analysis against STRM. For a standardized comparison framework, we selected models commonly integrated with CA, including CA-Markov (Daba & You, [2022](#)), LR-CA (Zhang et al., [2015](#)), RF-CA (Kamusoko & Gamba, [2015](#)), and ANN-CA (Yang et al., [2016](#)). Therefore, we employ Markov, Logistic Regression (LR), Random Forest (RF), and Artificial Neural Network (ANN) models to predict urban land quantity in Wuhan and compare these with the STRM model to evaluate performance. However, it's important to note that these widely used models lack the capability to make spatially explicit predictions of urban land quantity. They can only predict the total quantity of urban land in the study area annually. To ensure consistency in comparison, STRM uses the following equation to calculate the total quantity of urban land:

TABLE 4 Optimized parameters of the STRM model for predicting urban land demand in different predict periods.

Prediction period	Years	Lag period (k)	Neighborhood size (r)	Grid size (d)	Description
Near-term years	2000–2009	10	1	3	Taking 1990–1999 as the model training period, the urban land demand in the next 10 years is predicted.
Long-term year	2010–2017	10	1	5	Taking 1990–1999 as the model training period, the urban land demand in the next 11 to 17 years is predicted.

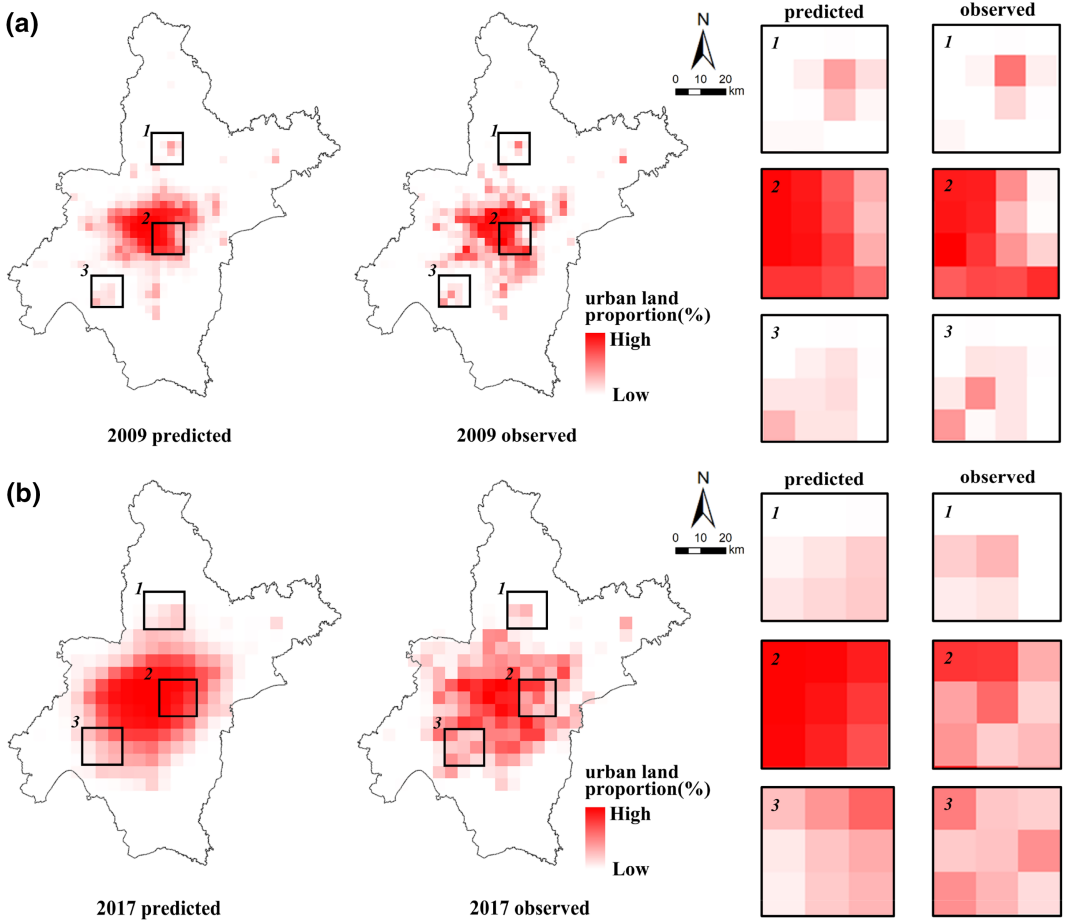


FIGURE 10 Comparison of predicted and observed values of optimal parameters. (a) Comparison of predicts for near-term year (2009) with observed values; (b) Comparison of predicts for long-term year (2017) with observed values.

$$Z_{i,t,d} = q_i \times (d^2 - S_w) \tag{4}$$

$$A_{t,d} = \sum_{i=1}^j Z_{i,t,d} \tag{5}$$

where $Z_{i,t,d}$ is the total quantity (area) of urban land in grid i with side length d in year t . q_i is the predicted value of urban land demand in grid i . S_w is the area of the water body in the grid. And j represents the total number of regular grids in the study area. Different grid sizes will result in different total number of grids in the study area. $A_{t,d}$ is the total amount of urban land in the study area in year t .

Conventional quantity prediction models were trained using data from 1990 to 1999 to predict urban land quantity annually from 2000 to 2017. STRM also uses this same time series data for its predictions, employing Equation (5) to calculate the annual urban land quantity. Figure 11 illustrates a comparison of the predictions from all models against actual observations. The annual demand totals predicted by STRM align most closely with observed values, displaying minimal discrepancies in annual distributions. The RF model follows closely but ranks second, with its predictions showing significant deviations from observed values in later years. The Markov model exhibits a wide range in its predicted annual demand totals, with substantial variances from observed values, especially in later years. In contrast, the LR and ANN models produce more compact predictions that diverge from the observed values.

In addition to Adjusted R^2 , we employ Mean Squared Error (MSE), Akaike Information Criterion (AICc), and Bayesian Information Criterion (BIC) to evaluate model accuracy and compare differences across models. Table 5 displays the calculation results for various models under multiple evaluation metrics from 2000 to 2017. Consistent with the statistical outcomes illustrated in Figure 11, STRM consistently achieves a higher mean Adjusted R^2 , along with lower MSE, AICc, and BIC values. Although the RF model excels at processing nonlinear data, its performance is limited by small sample sizes and local relationships within the data, which complicates noise management and results in significant errors, second only to those of STRM. The Markov model, known for its stable quantitative prediction capabilities, experiences a decline in performance in later years, resulting in increased prediction errors. Furthermore, the LR and ANN models display notably low accuracy, with LR particularly recording a significantly high MSE. The complex nonlinear dynamics inherent in the urban development process hinder the performance of LR, making it less suitable for long-term urban land demand predictions. Additionally, ANN's reliance on limited training data restricts its ability to capture broader patterns in urban land demand development, negatively impacting its prediction accuracy.

5.3 | Predicting future urban land demand to 2035

Using 1990 as the base year, this study utilized urban land demand data from Wuhan spanning from 1990 to 2017 as training data to predict urban land demand from 2018 to 2035 annually, using a lag period of 28 years

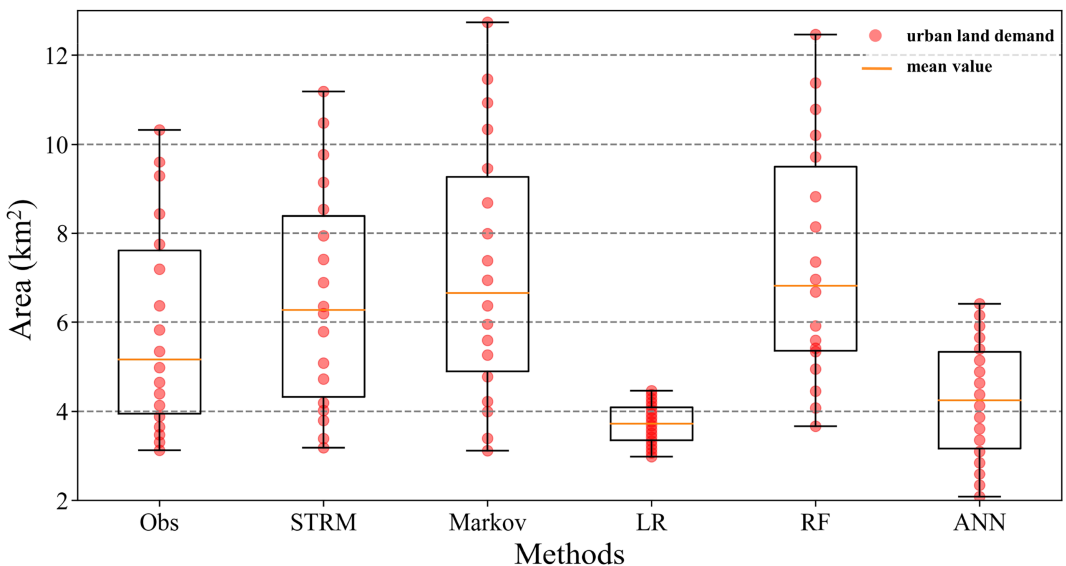


FIGURE 11 Descriptive statistics of results of different urban land demand prediction models.

TABLE 5 Evaluation results of different urban land demand prediction models.

Model	Average adjusted R^2	Average MSE	AICc	BIC
STRM	0.5374	4279.0914	168.3863	149.8382
Markov	-0.1864	20063.8064	207.3406	206.7924
LR	-0.9467	80526.0907	242.9809	220.4561
RF	0.3911	10746.9212	189.7128	166.1879
ANN	-0.5217	37648.5857	228.4212	211.7113

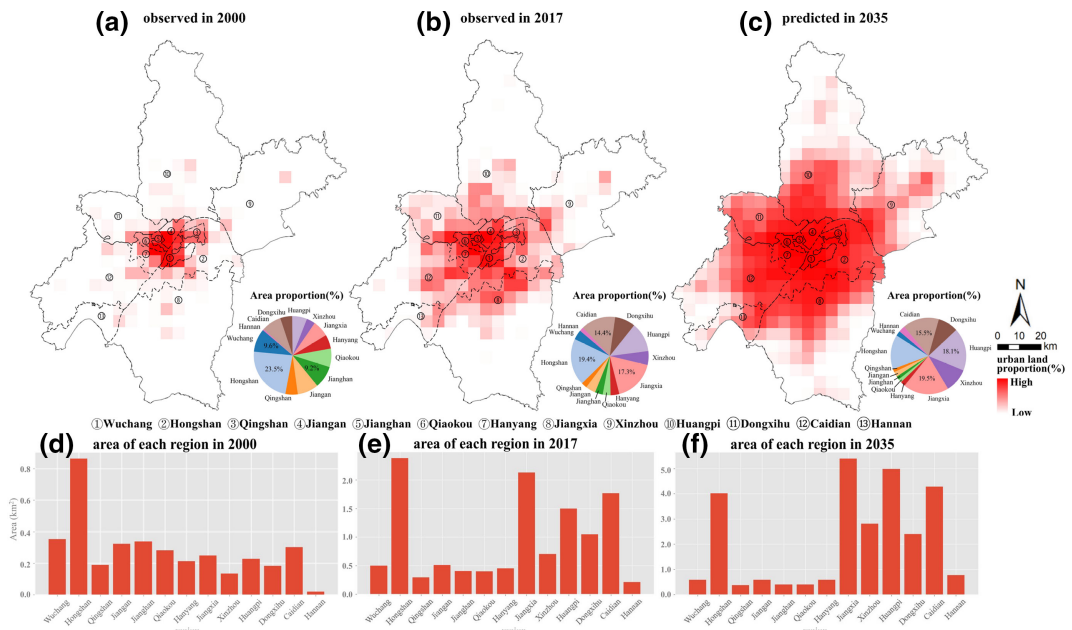


FIGURE 12 Observed urban land demand in 2000 and 2017, and predicted urban land demand in 2035. (a) Spatial observations of urban land demand in 2000; (b) Spatial observations of urban land demand in 2017; (c) Spatial predictions of urban land demand in 2035 under optimal parameters; (d–f) Urban land area of each region in Wuhan in 2000, 2017 and 2035.

($k = 28$), a neighborhood size of 1 ($r = 1$), and a grid size of 5 km ($d = 5$ km). [Figure 12c](#) displays the prediction results, providing a visual representation of the development trends and spatiotemporal distribution patterns of urban land demand in Wuhan. Observational data from the years 2000 and 2017 were used to summarize these trends. Additionally, urban land demand and grid size calculations were employed to determine the total area and proportion of urban land in each administrative district of Wuhan for the years 2000, 2017, and 2035. For each year, the top three regions by land proportion were highlighted with percentages, as shown in [Figure 12a–c](#).

[Figure 12](#) illustrates the continuous expansion of urban land in Wuhan from 2000 to 2035, with a distribution pattern that is concentrated around Wuchang, Hankou, and Hanyang and gradually decreases towards the suburban areas. Urban land in these central areas becomes increasingly concentrated, highlighting a clear pattern of urban-suburban integration. An analysis of the urban land area and proportions in each region from 2000 to 2035 reveals a consistent rise in total urban land, signifying the emergence of new development zones and suburbs as key growth areas. In 2000, the districts of Wuchang, Hongshan, and Jiangnan exhibited the highest proportions of urban land. Located at Wuhan's core, these older urban districts have traditionally served as transportation and commercial hubs, as depicted in [Figure 12a,d](#). As the urban expansion continues, newly developed urban areas stretch outward, reaching into the suburbs. By 2017, Hongshan, Caidian, and Jiangxia Districts had emerged as new urban growth areas, as shown in [Figure 12b,e](#) (Zhang et al., 2023). However, the central urban area of Wuhan, including districts like Wuchang and Jiang'an, is relatively constrained by limited land resources, leading to a gradual saturation of urban land demand. By 2035, it is anticipated that Jiangxia, Huangpi, and Caidian Districts will become new hubs of urban growth. These districts will serve as connectors between the central urban areas and suburban development, experiencing continual growth in urban land demand and further exemplifying spatial aggregation characteristics. This strategy is expected to significantly relieve population, transportation, and resource pressures in Wuhan's central city, aligning with the goals to establish a national-level central city.

6 | DISCUSSION

6.1 | Impact of parameters on model performance

This study confirms that within the defined parameter range, increasing the lag period significantly boosts the prediction performance of the model, demonstrating the positive impact of enhancing feature quantity on model efficacy. However, the inflection points observed in specific parameter combinations suggest that these could be attributed to the lag period. For instance, [Figure 13c,h,m](#) show that as the lag period increases, the inflection point for overall prediction accuracy moves progressively forward. This suggests that incorporating more input data from extended lag periods allows for longer effective predictions by the model, thereby reducing the accuracy degradation typically associated with rolling predictions. Owing to the inertial mechanism of urban development, development patterns often exhibit temporal similarities within certain periods (Kim et al., 2022; Tepe & Guldmann, 2017, 2020). The longer the lag period considered, the more effectively the model can learn the long-term trends of urban development and enhance prediction accuracy (Tepe & Safikhani, 2023). Additionally, as illustrated by [Figure 13j](#), there is a noticeable deceleration in the decline of prediction accuracy around 2010. Following the promulgation of the “Master Plan of Wuhan City (2010–2020)” in 2010, which aimed to balance the renewal of the main urban area with the expansion of its edges, the model’s consideration of neighborhood changes led to a concentration of urban land demand in existing urbanized areas. This adjustment not only captures shifts in policy but also aligns more closely with Wuhan’s policy direction.

On the other hand, the concept of spatial dependence, also known as the spatial neighborhood effect, suggests that “nearby locations exhibit similar spatial processes” (Mahtta et al., 2022). These findings are

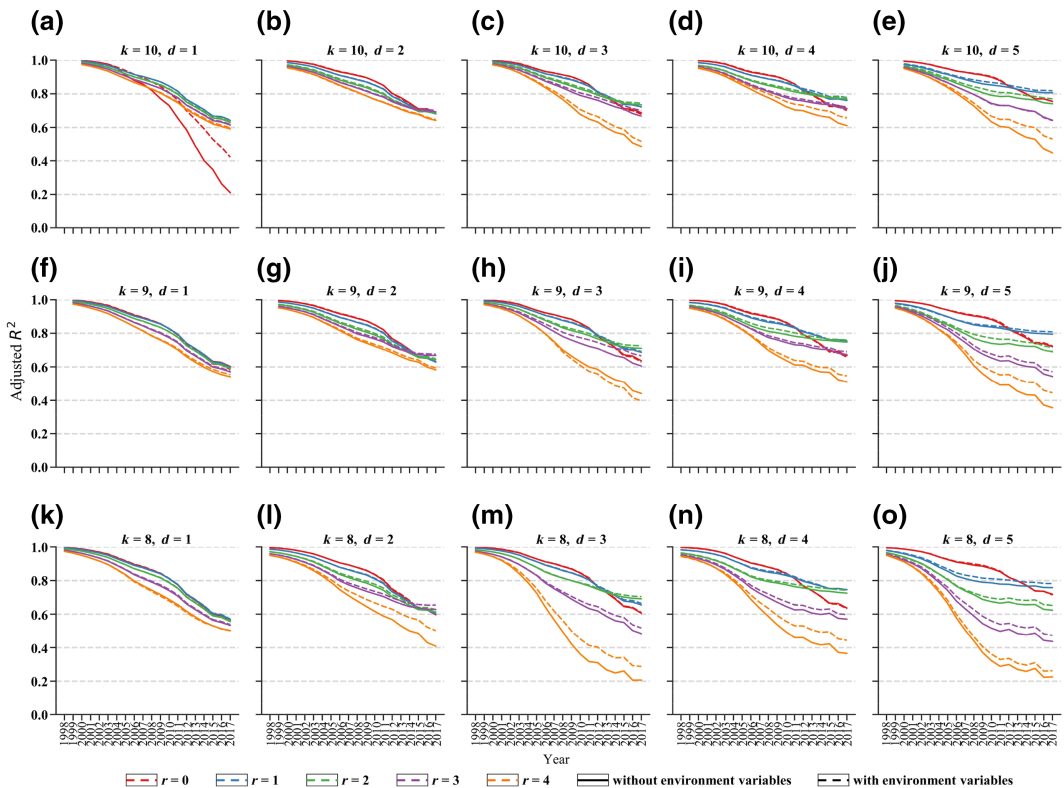


FIGURE 13 Model prediction accuracy under the combined influence of historical lag, neighborhood, and proximity. (a–o) Annual prediction accuracy under different spatiotemporal parameters.

consistent with the results presented in this study. Additionally, the study identifies marginal effects of neighborhood size on urban land demand prediction. As evidenced by [Figure 13c,i,o](#), with increasing neighborhood size, the prediction accuracy of STRM initially improves and then diminishes. Furthermore, the range of input data, determined by the neighborhood and grid size, mirrors this accuracy trend, suggesting that the spatial dependence of urban land demand is influenced by the scale effect. Prediction outcomes at different scales exhibit distinct patterns and trends, underscoring the variability in spatial processes (Ke et al., 2010; Lavalle et al., 2011). Incorporating considerations of neighborhood and spatial scale into STRM helps capture the edge and scale effects inherent in urban land demand. This approach not only enhances the model's ability to maximize the homogeneity of urban land demand but also more accurately simulates the processes and patterns that align with actual urban development dynamics.

Spatial interaction is influenced by the distance attenuation effect, where proximity between two locations directly increases the likelihood of their interaction (Guo et al., 2022; Kang et al., 2013; Onnela et al., 2011). In urban growth simulation studies, spatial proximity is often a critical factor (Mustafa et al., 2018; Sapena & Ruiz, 2021). For example, proximity measures are typically incorporated as model inputs in the definition of transformation rules for CA models, representing distance features (Liao et al., 2014; Tsai et al., 2015). Thus, it is essential to consider both the range of neighborhood demand and distance-driven variables within the grid. Moreover, in selecting parameters for this study, natural variables must also be considered, as they often serve as constraints for urban growth. Additionally, [Figure 13](#) illustrates that incorporating environmental variables can effectively enhance the prediction accuracy of STRM. Overall, the experiments in this study have demonstrated that historical development trends, neighborhood status, and proximity effectively characterize the spatiotemporal heterogeneity of urban land demand.

6.2 | Comparison of different mapping functions in STRM

This study further explored the robustness and generalizability of the rolling prediction process by comparing the deep forest model with random forest (RF) and artificial neural network (ANN), using identical parameters to extract spatiotemporal neighborhood information. [Figure 14](#) illustrates the predictive accuracy of the three models under various spatial parameters, focusing on the maximum lag year and the inclusion of environmental variables. Overall, the deep forest model consistently outperforms the others, demonstrating the highest predictive accuracy and effectively handling increased non-stationarity in larger neighborhoods. This ability enhances its usefulness in determining optimal spatiotemporal parameters for different scenarios. While the RF model maintains good overall accuracy, its results are relatively uniform across different neighborhoods and grid sizes, which restricts its effectiveness in analyzing the impacts of temporal dependence and spatial scale effects. In contrast, the predictive accuracy of the ANN model is markedly unsatisfactory, characterized by instability and significant deterioration over longer prediction periods. Utilizing the sensitivity analysis method applied in this study, optimal spatiotemporal parameter combinations for the three models were identified and compared, as shown in the last column of [Figure 14](#). The results reveal that the deep forest model not only exhibits high accuracy and stability but also outperforms the RF model, while the ANN model lags significantly behind. Consequently, the STRM, employing the deep forest model for mapping, proves to possess strong robust and generalization capabilities.

6.3 | Scenario simulation potentials and model generalizability

The complexity of urban development has led an increasing number of model developers to consider specific urban development scenarios. As demonstrated in the simulation results in [Appendix E](#), by fine-tuning the

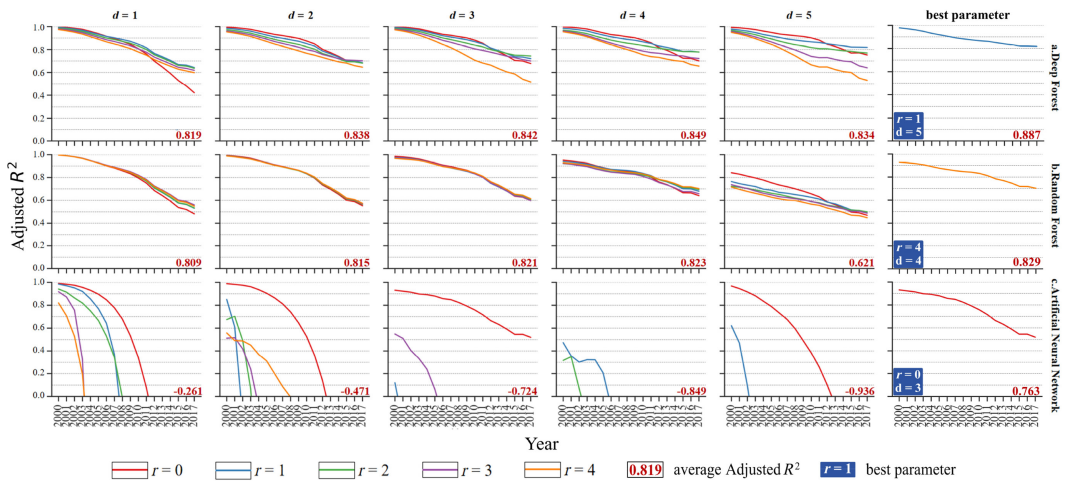


FIGURE 14 Accuracy comparison of rolling predict results from 2000 to 2017 by deep forest (a), RF (b) and ANN (c).

spatiotemporal parameters of STRM, modelers can effectively manage the spatiotemporal pattern of urban land demand, thus predicting it under various future urban development scenarios. Urban areas can generally be categorized by the degree of compactness into compact growth and dispersed growth. The size of the neighborhood in STRM influences the spatial compactness of future urban land demand, as illustrated in Figure S5 in Appendix E, larger neighborhood sizes tend to promote more compact growth.

Urban areas can also be historically classified into satellite urban areas (or new development zones) and those with a long history. Predicting future urban land demand for these categories can be managed by adjusting the lag period, as shown in Figure S6. Moreover, special urban development scenarios, such as those experiencing rapid population growth or high agglomeration, should be considered. Integrating spatialized population distribution data into environmental variables can help regulate the spatial distribution of urban land demand relative to these variables. It is important to note that STRM is open and flexible. This paper confirms the suitability of specific parameters and the effectiveness of environmental variables in enhancing STRM's performance. Looking ahead, we aim to acquire more robust data to enhance the model's feasibility for predicting demand in different urban development scenarios.

Numerous studies have highlighted the significance of distance variables in urban development (Seto & Fragkias, 2005; Vizzari & Sigura, 2015; Xu et al., 2007), and incorporating environmental variables generally enhances the prediction accuracy of STRM, as shown in Figure 13. Additionally, employing temporal series data to model urban development patterns has become a prevalent approach in urban growth studies (Ferdous & Bhat, 2013; Yang et al., 2020). While STRM relies on fitting historical data to predict urban land demand, unforeseen events such as natural disasters or significant demographic shifts, like those during COVID-19, can challenge the model's effectiveness. Reflecting this, STRM can adapt to special historical change trajectories, such as those driven by policy shifts, as indicated in Figure 13 around the year 2010. This adaptability not only allows for the capture of structural changes in urban development over time but also aids in refining parameters to better align with urban land demand. These studies lend theoretical and practical support to the feasibility and applicability of STRM.

To further validate STRM's effectiveness, an additional experiment was conducted in Jinan, Shandong Province, where economic growth and urban development have been somewhat slower compared to Wuhan. The same methodologies employed in Wuhan were applied to verify STRM's optimal parameters in Jinan. The results, detailed in Appendix F, show that STRM achieved an Adjusted R^2 of 0.89 in 2017, with an average Adjusted R^2 of 0.94 from 2000 to 2017. This high level of prediction accuracy underscores the model's generalizability.

7 | CONCLUSION

This study introduces a dynamic spatiotemporal rolling prediction model (STRM) for year-by-year spatially explicit prediction of urban land demand. STRM integrates spatiotemporal lag effects and proximity considerations to effectively delineate the heterogeneity of urban land demand. This allows for dynamic analysis of parameter sensitivity and proximity effects across various cities, providing a robust approach for identifying optimal spatiotemporal parameters for predicting urban land demand. Additionally, STRM's rolling prediction method relies solely on historical demand and static variables for future annual predictions, adeptly addressing the challenge of predicting future urban land demand without variable environment data or specific future characteristics.

Experimental results demonstrate that STRM effectively predicts urban land demand over the next 17 years, achieving an average Adjusted R^2 of 0.89 from 2000 to 2017, with a 2017 Adjusted R^2 of 0.81. As groundbreaking research, STRM simplifies complex modeling and offers a higher resolution method for predicting spatiotemporal urban land demand. Analyses of parameter and structural sensitivity reveal that lag period, neighborhood size, and proximity significantly influence STRM performance, highlighting patterns that affect prediction accuracy. Prediction accuracy correlates positively with the length of the historical lag period, shows marginal effects from neighborhood size, and generally improves with the inclusion of environment variables.

STRM's predictions for Wuhan in 2035 suggest that urban land demand will continue to increase, with the central urban area nearing saturation. Jiangxia, Huangpi, and Caidian districts are identified as the city's new growth areas. This study fills a crucial gap in spatiotemporal prediction research for urban land demand, offering a practical tool that utilizes historical data and essential distance-driven variables to inform urban growth potential and effective land resource management. This insight supports future urban planning and addresses various urban challenges.

While this study confirms STRM's effectiveness within a limited parameter scope, future research should expand these parameters to verify the model's applicability across diverse urban contexts. Additionally, the limitation of non-spatializable socioeconomic data might restrict the model's ability to predict urban land demand under varying urban development scenarios. Despite these areas for enhancement, STRM's novel approach provides a fresh strategy for examining urban development dynamics.

ACKNOWLEDGMENTS

This work was supported by the National Natural Science Foundation of China (NO.42101275), the Fundamental Research Funds for the Central Universities, China University of Geosciences (CUGL170408, CUGGG-2021), and the Provincial Natural Science Foundation of Hubei, China (NO. 2023AFB651).

CONFLICT OF INTEREST STATEMENT

The authors report there are no competing interests to declare.

DATA AVAILABILITY STATEMENT

The data that support the findings of this study are available from the corresponding author upon reasonable request.

ORCID

Yingjian Ren  <https://orcid.org/0009-0007-9658-3106>

Zhong Zhang  <https://orcid.org/0000-0003-3002-4831>

REFERENCES

Ahasan, R., & Güneralp, B. (2022). Transportation in urban land change models: A systematic review and future directions. *Journal of Land Use Science*, 17(1), 351–367. <https://doi.org/10.1080/1747423X.2022.2086639>

- Aquilué, N., De Cáceres, M., Fortin, M., Fall, A., & Brotons, L. (2017). A spatial allocation procedure to model land-use/land-cover changes: Accounting for occurrence and spread processes. *Ecological Modelling*, 344, 73–86. <https://doi.org/10.1016/j.ecolmodel.2016.11.005>
- Arsanjani, J. J., Helbich, M., Kainz, W., & Bolorani, A. D. (2013). Integration of logistic regression, Markov chain and cellular automata models to simulate urban expansion. *International Journal of Applied Earth Observation and Geoinformation*, 21, 265–275. <https://doi.org/10.1016/j.jag.2011.12.014>
- Balmaceda, B., & Fuentes, M. (2016). Cities and methods from complexity science. *Journal of Systems Science and Complexity*, 5, 1177–1186. <https://doi.org/10.1007/s11424-016-6084-2>
- Batty, M., Bettencourt, L. M. A., & Kirley, M. (2019). Understanding coupled urban natural dynamics as the key to sustainability: The example of the galapagos. *Urban Galapagos*, 43(4), 23–41. https://doi.org/10.1007/978-3-319-99534-2_3
- Bhat, C. R., Dubey, S. K., Alam, M. J., & Khushefati, W. H. (2015). A new spatial multiple discrete-continuous modeling approach to land use change analysis. *Journal of Regional Science*, 55(5), 801–841. <https://doi.org/10.1111/jors.12201>
- Castella, J.-C., & Verburg, P. H. (2007). Combination of process-oriented and pattern-oriented models of land-use change in a mountain area of Vietnam. *Ecological Modelling*, 202, 410–420. <https://doi.org/10.1016/j.ecolmodel.2006.11.011>
- Chen, Y., Li, X., Liu, X., & Ai, B. (2014). Modeling urban land-use dynamics in a fast-developing city using the modified logistic cellular automaton with a patch-based simulation strategy. *International Journal of Geographical Information Science*, 28, 234–255. <https://doi.org/10.1080/13658816.2013.831868>
- Chen, Y., Li, X., Liu, X., Zhang, Y., & Huang, M. (2019). Tele-connecting China's future urban growth to impacts on ecosystem services under the shared socioeconomic pathways. *Science of the Total Environment*, 652, 765–779. <https://doi.org/10.1016/j.scitotenv.2018.10.283>
- China, S. S. B. (2010). China statistical yearbook, 2010.
- China, S. S. B. (2020). China statistical yearbook, 2020.
- Cilliers, P., van Vuuren, J. H., & van Heerden, Q. (2021). A framework for modelling spatiotemporal informal settlement growth prediction. *Computers, Environment and Urban Systems*, 90, 101707. <https://doi.org/10.1016/j.compenvurb.2021.101707>
- Cunha, E. R. D., Santos, C. A. G., Silva, R. M. D., Bacani, V. M., & Pott, A. (2021). Future scenarios based on a CA-Markov land use and land cover simulation model for a tropical humid basin in the Corrado/Atlantic forest ecotone of Brazil. *Land Use Policy*, 101, 105–141. <https://doi.org/10.1016/j.landusepol.2020.105048>
- Daba, M. H., & You, S. (2022). Quantitatively assessing the future land-use/land-cover changes and their driving factors in the upper stream of the Awash River based on the CA-Markov model and their implications for water resources management. *Sustainability*, 14(3), 15–38. <https://doi.org/10.3390/su14031538>
- Deng, Y., & Srinivasan, S. (2016). Urban land use change and regional access: A case study in Beijing, China. *Habitat International*, 51, 103–113. <https://doi.org/10.1016/j.habitatint.2015.09.007>
- Engelen, G., Lavallo, C., Barredo, J. I., Meulen, M., & White, R. (2007). The Moland modelling framework for urban and regional land-use dynamics. In E. Koomen, J. Stillwell, A. Bakema, & H. J. Scholten (Eds.), *Modelling land-use change: Progress and applications* (pp. 297–320). Springer. https://doi.org/10.1007/978-1-4020-5648-2_16
- Ferdous, N., & Bhat, C. R. (2013). A spatial panel ordered-response model with application to the analysis of urban land-use development intensity patterns. *Journal of Geographical Systems*, 15(1), 1–29. <https://doi.org/10.1007/s10109-012-0165-0>
- Fisher-Gewirtzman, D., & Blumenfeld-Liberthal, E. (2013). An agent-based model for simulating urban morphology: Sachnin as a case study. *Survey Review*, 44, 162–167. <https://doi.org/10.1179/1752270612Y.0000000016>
- Fu, X., Wang, X., & Yang, Y. J. (2018). Deriving suitability factors for CA-Markov land use simulation model based on local historical data. *Journal of Environmental Management*, 206, 10–19. <https://doi.org/10.1016/j.jenvman.2017.10.001>
- Gao, J., Gong, J., Yang, J., Li, J., & Li, S. (2022). Measuring spatial connectivity between patches of the heat source and sink (SCSS): A new index to quantify the heterogeneity impacts of landscape patterns on land surface temperature. *Landscape and Urban Planning*, 217, 104260. <https://doi.org/10.1016/j.landurbplan.2021.104260>
- Gong, P., Li, X., Wang, J., Bai, Y., Chen, B., Hu, T., Liu, X., Xu, B., Yang, J., Zhang, W., & Zhou, Y. (2020). Annual maps of global artificial impervious area (GAIA) between 1985 and 2018. *Remote Sensing of Environment*, 236, 111510. <https://doi.org/10.1016/j.rse.2019.111510>
- Goodchild, M. F. (2004). The validity and usefulness of laws in geographic information science and geography. *Annals of the Association of American Geographers*, 94(2), 300–303. <https://doi.org/10.1111/j.1467-8306.2004.09402007.x>
- Guo, H., Zhang, W. Y., Du, H. D., Kang, C., & Liu, Y. (2022). Understanding China's urban system evolution from web search index data. *EPJ Data Science*, 11(1), 20. <https://doi.org/10.1140/epjds/s13688-022-00332-y>
- Harris, P., Comber, A., & Tsutsumida, N. (2017). Specifying regression models for spatiotemporal data sets.

- He, J., Li, X., Yao, Y., Hong, Y., & Jinbao, Z. (2018). Mining transition rules of cellular automata for simulating urban expansion by using the deep learning techniques. *International Journal of Geographical Information Science*, 32, 2076–2097. <https://doi.org/10.1080/13658816.2018.1480783>
- Hu, Z., & Lo, C. P. (2007). Modeling urban growth in Atlanta using logistic regression. *Computers, Environment and Urban Systems*, 31(6), 667–688. <https://doi.org/10.1016/j.compenvurbsys.2006.11.001>
- Huang, B., Zhang, L., & Wu, B. (2009). Spatiotemporal analysis of rural-urban land conversion. *International Journal of Geographical Information Science*, 23(3), 379–398. <https://doi.org/10.1080/13658810802119685>
- Huang, Q., Zhang, H., Vliet, J., Ren, Q., Wang, R. Y., Du, S., Liu, Z., & He, C. (2021). Patterns and distributions of urban expansion in global watersheds. *Earth's Futures*, 9(8), e2020EF001900. <https://doi.org/10.1029/2020EF001900>
- Iacono, M., Levinson, D., & El-Geneidy, A. (2008). Models of transportation and land use change: A guide to the territory. *Journal of Planning Literature*, 22(4), 323–340. <https://doi.org/10.1177/0885412207314010>
- Kamuso, C., & Gamba, J. (2015). Simulating urban growth using a random forest – cellular automata (RF-CA) model. *Inspire International Journal of Geo-Information*, 4, 447–470. <https://doi.org/10.3390/ijgi4020447>
- Kang, C. G., Zhang, Y., Ma, X. J., & Liu, Y. (2013). Inferring properties and revealing geographical impacts of intercity mobile communication network of China using a subnet data set. *International Journal of Geographical Information Science*, 27(3), 431–448. <https://doi.org/10.1080/13658816.2012.689838>
- Ke, X., Deng, X., & He, S. (2010). Scale sensitivity and its causality for geo-cellular automata modelling. *Geographical Research*, 29(5), 863–872. <https://doi.org/10.11821/yj2010050010>
- Ke, X., Qi, L., & Zeng, C. (2015). A partitioned and asynchronous cellular automata model for urban growth simulation. *International Journal of Geographical Information Science*, 30(4), 637–659. <https://doi.org/10.1080/13658816.2015.1099656>
- Ke, X., van Vliet, J., Zhou, T., Verburg, P. H., Zheng, W., & Liu, X. (2018). Direct and indirect loss of natural habitat due to built-up area expansion: A model-based analysis for the city of Wuhan, China. *Land Use Policy*, 74, 231–239. <https://doi.org/10.1016/j.landusepol.2018.03.001>
- Kim, Y., Safikhani, A., & Tepe, E. (2022). Machine learning application to spatiotemporal modeling of urban growth. *Computers, Environment and Urban Systems*, 94, 101801. <https://doi.org/10.1016/j.compenvurbsys.2022.101801>
- Lauf, S., Haase, D., Hostert, P., Lakes, T., & Kleinschmit, B. (2012). Uncovering land-use dynamics driven by human decision-making—a combined model approach using cellular automata and system dynamics. *Environmental Modelling & Software*, 27, 71–82. <https://doi.org/10.1016/j.envsoft.2011.09.004>
- Lavalle, C., Baranzelli, C., e Silva, F. B., Mubareka, S., Gomes, C. R., Koomen, E., & Hilferink, M. (2011). A high-resolution land use/cover modelling framework for Europe: Introducing the EU-CLUEScanner100 model. *Computational Science and Its Applications – ICCSA 2011, Santander, Spain, June 20–23, 2011*. https://doi.org/10.1007/978-3-642-21928-3_5
- Li, X., & Yeh, A. (2001). Calibration of cellular automata by using neural networks for the simulation of complex urban systems. *Environment and Planning A: Economy and Space*, 33, 1445–1462. <https://doi.org/10.1068/a33210>
- Li, Y., Lin, A., Wu, H., Wu, X., Cen, L., Liu, H., & Jiang, Z. (2022). Refined simulation of urban land use change with emphasis on spatial scale effect. *Acta Geographica Sinica*, 77(11), 2738–2756. <https://doi.org/10.11821/dlxb202211004>
- Liang, X., Guan, Q., Clarke, K. C., Liu, S., Wang, B., & Yao, Y. (2021). Understanding the drivers of sustainable land expansion using a patch-generating land use simulation (PLUS) model: A case study in Wuhan, China. *Computers, Environment and Urban Systems*, 85, 101569. <https://doi.org/10.1016/j.compenvurbsys.2020.101569>
- Liao, F. H. F., & Wei, Y. H. D. (2014). Modeling determinants of urban growth in Dongguan, China: A spatial logistic approach. *Stochastic Environmental Research and Risk Assessment*, 28(4), 801–816. <https://doi.org/10.1007/s00477-012-0620-y>
- Liao, J., Tang, L., Shao, G., Su, X., Chen, D., & Xu, T. (2016). Incorporation of extended neighborhood mechanisms and its impact on urban land-use cellular automata simulations. *Environmental Modelling & Software*, 75, 163–175. <https://doi.org/10.1016/j.envsoft.2015.10.013>
- Liao, J. F., Tang, L. N., Shao, G. F., Qiu, Q. Y., Wang, C. P., Zheng, S. N., & Su, X. D. (2014). A neighbor decay cellular automata approach for simulating urban expansion based on particle swarm intelligence. *International Journal of Geographical Information Science*, 28, 720–738. <https://doi.org/10.1080/13658816.2013.869820>
- Liu, D., Zheng, X., & Wang, H. (2020). Land-use simulation and decision-support system (LandSDS): Seamlessly integrating system dynamics, agent-based model, and cellular automata. *Ecological Modelling*, 417, 108924. <https://doi.org/10.1016/j.ecolmodel.2020.108946>
- Liu, M., Chen, H., Qi, L., & Chen, C. (2023). LUCC simulation based on RF-CNN-LSTM-CA model with high-quality seed selection iterative algorithm. *Applied Sciences*, 13, 3407. <https://doi.org/10.3390/app13063407>
- Liu, X., Xun, L., Xia, L., Xiaocong, X., Jinpei, O., Yimin, C., Shaoying, L., Shaojian, W., & Fengsong, P. (2017). A future land use simulation model (FLUS) for simulating multiple land use scenarios by coupling human and natural effects. *Landscape and Urban Planning*, 168, 94–116. <https://doi.org/10.1016/j.landurbplan.2017.09.019>

- Losiri, C., Nagai, M., Ninsawat, S., & Shrestha, R. (2016). Modeling urban expansion in Bangkok metropolitan region using demographic-economic data through cellular automata-Markov chain and multi-layer perceptron-Markov chain models. *Sustainability*, 8, 686. <https://doi.org/10.3390/su8070686>
- Mahtta, R., Fragkias, M., Güneralp, B., Mahendra, A., Reba, M., Wentz, E. A., & Seto, K. C. (2022). Urban land expansion: The role of population and economic growth for 300+ cities. *Urban Sustainability*, 2, 5. <https://doi.org/10.1038/s42949-022-00048-y>
- Meentemeyer, R. K., Tang, W. W., Dorning, M. A., Vogler, J. B., Cunniffe, N. J., & Shoemaker, D. A. (2013). FUTURES: Multilevel simulations of emerging urban-rural landscape structure using a stochastic patch-growing algorithm. *Annals of the Association of American Geographers*, 103, 785–807. <https://doi.org/10.1080/00045608.2013.779503>
- Morrill, R. L. (1970). The shape of diffusion in space and time. *Economic Geography*, 46(sup1), 259–268. <https://doi.org/10.2307/143143>
- Munroe, D. K., & Müller, D. (2007). Issues in spatially explicit statistical land-use/cover change (LUCC) models: Examples from western Honduras and the central highlands of Vietnam. *Land Use Policy*, 24(3), 521–530. <https://doi.org/10.1016/j.landusepol.2005.09.007>
- Mustafa, A., Saadi, I., Cools, M., & Teller, J. (2018). A time Monte Carlo method for addressing uncertainty in land-use change models. *International Journal of Geographical Information Science*, 32, 2317–2333. <https://doi.org/10.1080/13658816.2018.1508689>
- Nahuelhual, L., Carmona, A., Lara, A., Echeverría, C., & González, M. E. (2012). Land-cover change to forest plantations: Proximate causes and implications for the landscape in south-central Chile. *Landscape and Urban Planning*, 107(1), 12–20. <https://doi.org/10.1016/j.landurbplan.2012.04.006>
- Noszczyk, T. (2018). A review of approaches to land use changes modeling. *Human and Ecological Risk Assessment: An International Journal*, 25(6), 1377–1405. <https://doi.org/10.1080/10807039.2018.1458593>
- Onnela, J. P., Arbesman, S., González, M. C., Barabási, A. L., & Christakis, N. A. (2011). Geographic constraints on social network groups. *PLoS One*, 6(4), e16939. <https://doi.org/10.1371/journal.pone.0016939>
- Osman, T., Divigalpitiya, P., & Arima, T. (2016). Using the SLEUTH urban growth model to simulate the impacts of future policy scenarios on land use in the Giza governorate, greater Cairo metropolitan region. *International Journal of Urban Sciences*, 20, 407–426. <https://doi.org/10.1080/12265934.2016.1182062>
- Ou, J., Liu, X., Li, X., Chen, Y., & Li, J. (2017). Quantifying spatiotemporal dynamics of urban growth modes in metropolitan cities of China: Beijing, Shanghai, Tianjin, and Guangzhou. *Journal of Urban Planning and Development*, 143(1), 149–177. <https://doi.org/10.1061/UP.1943-5444.0000352>
- Qin, Y. S., & Lei, Q. Z. (2021). Empirical likelihood for mixed regressive, spatial autoregressive model based on GMM. *Sankhya A: The Indian Journal of Statistics*, 83, 353–378. <https://doi.org/10.1007/s13171-019-00190-3>
- Sapena, M., & Ruiz, L. A. (2021). Identifying urban growth patterns through land-use/land-cover spatio-temporal metrics: Simulation and analysis. *International Journal of Geographical Information Science*, 35, 375–396. <https://doi.org/10.1080/13658816.2020.1817463>
- Schneider, A., & Woodcock, C. E. (2008). Compact, dispersed, fragmented, extensive? A comparison of urban growth in twenty-five global cities using remotely sensed data, pattern metrics and census information. *Urban Studies*, 45(3), 659–692. <https://doi.org/10.1177/0042098007087343>
- Seto, K. C., & Fragkias, M. (2005). Quantifying spatiotemporal patterns of urban land-use change in four cities of China with time series landscape metrics. *Landscape Ecology*, 20, 871–888. <https://doi.org/10.1007/s10980-005-5238-8>
- Seto, K. C., Güneralp, B., & Hutyra, L. R. (2012). Global forecasts of urban expansion to 2030 and direct impacts on biodiversity and carbon pools. *Proceedings of the National Academy of Sciences of the United States of America*, 109(40), 16083–16088. <https://doi.org/10.1073/pnas.1211658109>
- Stanilov, K., & Batty, M. (2011). Exploring the historical determinants of urban growth patterns through cellular automata. *Transactions in GIS*, 15(3), 253–271. <https://doi.org/10.1111/j.1467-9671.2011.01261.x>
- Tang, L., Ke, X., Chen, Y., Wang, L., Zhou, Q., Zheng, W., & Xiao, B. (2021). Which impacts more seriously on natural habitat loss and degradation? Cropland expansion or urban expansion? *Land Degradation & Development*, 32, 946–964. <https://doi.org/10.1002/ldr.3790>
- Tepe, E. (2023). History, neighborhood, and proximity as factors of land-use change: A dynamic spatial regression model. *Environment and Planning B: Urban Analytics and City Science*, 51(1), 439–472. <https://doi.org/10.1177/23998083231164397>
- Tepe, E., & Guldmann, J.-M. (2017). Spatial and temporal modeling of parcel-level land dynamics. *Computers, Environment and Urban Systems*, 64, 204–214. <https://doi.org/10.1016/j.compenvurbusys.2017.02.005>
- Tepe, E., & Guldmann, J.-M. (2020). Spatiotemporal multinomial autologistic modeling of land-use change: A parcel-level approach. *Environment and Planning B: Urban Analytics and City Science*, 47(3), 473–488. <https://doi.org/10.1177/2399808318786511>
- Tepe, E., & Safikhani, A. (2023). Spatio-temporal modeling of parcel-level land-use changes using machine learning methods. *Sustainable Cities and Society*, 90, 104390. <https://doi.org/10.1016/j.scs.2023.104390>

- Tobler, W. (2004). On the first law of geography: A reply. *Annals of the Association of American Geographers*, 94, 304–310. <https://doi.org/10.1111/j.1467-8306.2004.09402009.x>
- Tsai, Y., Zia, A., Koliba, C., Bucini, G., Guilbert, J., & Beckage, B. (2015). An interactive land use transition agent-based model (ILUTABM): Endogenizing human-environment interactions in the Western Missisquoi watershed. *Land Use Policy*, 49, 161–176. <https://doi.org/10.1016/j.landusepol.2015.07.008>
- van Vliet, J., Eitelberg, D. A., & Verburg, P. H. (2017). A global analysis of land take in cropland areas and production displacement from urbanization. *Global Environmental Change*, 43, 107–115. <https://doi.org/10.1016/j.gloenvcha.2017.02.001>
- Verburg, P. H., Zhang, Y., & Zhao, S. (2003). CLUE-S and its application for simulating temporal and spatial change of land use in Naiman banner. *Journal of Natural Resources*, 18, 310–318. <https://doi.org/10.11849/zrzyxb.2003.03.008>
- Vizzari, M., & Sigura, M. (2015). Landscape sequences along the urban–rural–natural gradient: A novel geospatial approach for identification and analysis. *Landscape and Urban Planning*, 140, 42–55. <https://doi.org/10.1016/j.LANDURBPLAN.2015.04.001>
- Waddell, P. (2007). UrbanSim: Modeling urban development for land use, transportation, and environmental planning. *Journal of the American Planning Association*, 68, 297–314. <https://doi.org/10.1080/01944360708977976>
- Wang, Q., & Wang, H. (2022). An integrated approach of logistic-MCE-CA-Markov to predict the land use structure and their micro-spatial characteristics analysis in Wuhan metropolitan area, Central China. *Environmental Science and Pollution Research International*, 29(20), 30030–30053. <https://doi.org/10.1007/s11356-021-17750-6>
- Wu, F. (1997). Changing spatial distribution and determinants of land development in Chinese cities in the transition from a centrally planned economy to a socialist market economy: A case study of Guangzhou. *Urban Studies*, 11, 1851–1879. <https://doi.org/10.1080/0042098975286>
- Xu, C., Liu, M., Zhang, C., An, S., Yu, W., & Chen, J. M. (2007). The spatiotemporal dynamics of rapid urban growth in the Nanjing metropolitan region of China. *Landscape Ecology*, 22, 925–937. <https://doi.org/10.1007/s10980-007-9079-5>
- Xu, Q., Wang, Q., Liu, J., & Liang, H. (2021). Simulation of land-use changes using the partitioned ANN-CA model and considering the influence of land-use change frequency. *ISPRS International Journal of Geo-Information*, 10, 346. <https://doi.org/10.3390/ijgi10050346>
- Xu, Y., Olmos, L. E., Abbar, S., & Gonzalez, M. C. (2020). Deconstructing laws of accessibility and facility distribution in cities. *Science Advances*, 6, 1–24. <https://doi.org/10.1126/sciadv.abb4112>
- Yang, J., Sun, Y., Zhu, J., & Song, S. (2023). Simulating urban land-use change based on the multi-hierarchical planning–environment interaction process. *Transactions in GIS*, 27, 152–175. <https://doi.org/10.1111/tgis.13015>
- Yang, J., Tang, W., Gong, J., Shi, R., Zheng, M., & Dai, Y. (2023). Simulating urban expansion using cellular automata model with spatiotemporally explicit representation of urban demand. *Landscape and Urban Planning*, 231, 104640. <https://doi.org/10.1016/j.landurbplan.2022.104640>
- Yang, J. X., Gong, J., Tang, W. W., & Liu, C. (2020). Patch-based cellular automata model of urban growth simulation: Integrating feedback between quantitative composition and spatial configuration. *Computers, Environment and Urban Systems*, 79, 17. <https://doi.org/10.1016/j.compenvurbsys.2019.101418>
- Yang, X., Chen, R., & Zheng, X. Q. (2016). Simulating land use change by integrating ANN-CA model and landscape pattern indices. *Geomatics, Natural Hazards and Risk*, 7, 918–932. <https://doi.org/10.1080/19475705.2014.1001797>
- Ye, H., He, X., Song, Y., Li, X., Zhang, G., Lin, T., & Xiao, L. (2015). A sustainable urban form: The challenges of compactness from the viewpoint of energy consumption and carbon emission. *Energy and Buildings*, 93, 90–98. <https://doi.org/10.1016/j.enbuild.2015.02.011>
- Zhai, Y., Yao, Y., Guan, Q., Liang, X., Li, X., Pan, Y., Yue, H., Yuan, Z., & Zhou, J. (2020). Simulating urban land use change by integrating a convolutional neural network with vector-based cellular automata. *International Journal of Geographical Information Science*, 34, 1475–1499. <https://doi.org/10.1080/13658816.2020.1744175>
- Zhang, B., Hu, S., Wang, H., & Zeng, H. (2023). A size-adaptive strategy to characterize spatially heterogeneous neighborhood effects in cellular automata simulation of urban growth. *Landscape and Urban Planning*, 229, 104604. <https://doi.org/10.1016/j.landurbplan.2022.104604>
- Zhang, Y., Qiao, J., Wu, B., Jiang, W., Xu, X., & Hu, G. (2015). Simulation of oil spill using logistic-regression CA model. 2015 23rd International Conference on Geoinformatics. <https://doi.org/10.1109/GEOINFORMATICS.2015.7378559>
- Zhang, Z., Li, X., Liu, X., & Zhao, K. (2024). Dynamic simulation and projection of land use change using system dynamics model in the Chinese Tianshan mountainous region, central Asia. *Ecological Modelling*, 487, 110564. <https://doi.org/10.1016/j.ecolmodel.2023.110564>
- Zhou, Y., Huang, X., Zhong, T., Chen, Y., Yang, H., Chen, Z., Xu, G., Niu, L., & Li, H. (2020). Can annual land use plan control and regulate construction land growth in China? *Land Use Policy*, 99, 105026. <https://doi.org/10.1016/j.landusepol.2020.105026>
- Zhou, Z., & Feng, J. (2019). Deep forest. *National Science Review*, 6, 74–86. <https://doi.org/10.1093/nsr/nwy108>

SUPPORTING INFORMATION

Additional supporting information can be found online in the Supporting Information section at the end of this article.

How to cite this article: Ren, Y., Yang, J., Shen, Y., Wang, L., Zhang, Z., & Zhao, Z. (2024). Multidimensional effects of history, neighborhood, and proximity on urban land growth: A dynamic spatiotemporal rolling prediction model (STRM). *Transactions in GIS*, 00, 1–29. <https://doi.org/10.1111/tgis.13224>